Progenitor identification and SARS-CoV-2 infection in human distal lung organoids

Received: 8 November 2017

Accepted: 18 November 2020

Accelerated Article Preview Published online 25 November 2020

Cite this article as: Salahudeen, A. A. et al. Progenitor identification and SARS-CoV-2 infection in human distal lung organoids. *Nature* https://doi.org/10.1038/s41586-020-3014-1 (2020).

Ameen A. Salahudeen, Shannon S. Choi, Arjun Rustagi, Junjie Zhu, Vincent van Unen, Sean M. de la O, Ryan A. Flynn, Mar Margalef-Català, António J. M. Santos, Jihang Ju, Arpit Batish, Tatsuya Usui, Grace X. Y. Zheng, Caitlin E. Edwards, Lisa E. Wagar, Vincent Luca, Benedict Anchang, Monica Nagendran, Khanh Nguyen, Daniel J. Hart, Jessica M. Terry, Phillip Belgrader, Solongo B. Ziraldo, Tarjei S. Mikkelsen, Pehr B. Harbury, Jeffrey S. Glenn, K. Christopher Garcia, Mark M. Davis, Ralph S. Baric, Chiara Sabatti, Manuel R. Amieva, Catherine A. Blish, Tushar J. Desai & Calvin J. Kuo

This is a PDF file of a peer-reviewed paper that has been accepted for publication. Although unedited, the content has been subjected to preliminary formatting. Nature is providing this early version of the typeset paper as a service to our authors and readers. The text and figures will undergo copyediting and a proof review before the paper is published in its final form. Please note that during the production process errors may be discovered which could affect the content, and all legal disclaimers apply.

Progenitor identification and SARS-CoV-2 infection in human distal lung organoids

https://doi.org/10.1038/s41586-020-3014-1

Received: 8 November 2017

Accepted: 18 November 2020

Published online: 25 November 2020

Ameen A. Salahudeen[1,18,19], Shannon S. Choi[1,19], Arjun Rustagi[2], Junjie Zhu[3], Vincent van Unen[4,9], Sean M. de la O[1], Ryan A. Flynn[5], Mar Margalef-Català[6], António J. M. Santos[1], Jihang Ju[1], Arpit Batish[1], Tatsuya Usui[1], Grace X. Y. Zheng[7], Caitlin E. Edwards[8], Lisa E. Wagar[4,9], Vincent Luca[10], Benedict Anchang[11], Monica Nagendran[12], Khanh Nguyen[13], Daniel J. Hart[1], Jessica M. Terry[7], Phillip Belgrader[7], Solongo B. Ziraldo[7], Tarjei S. Mikkelsen[7], Pehr B. Harbury[14], Jeffrey S. Glenn[4,13], K. Christopher Garcia[10,15], Mark M. Davis[4,9,15], Ralph S. Baric[8,16], Chiara Sabatti[11], Manuel R. Amieva[4,6], Catherine A. Blish[2,17]✉, Tushar J. Desai[12]✉ & Calvin J. Kuo[1]✉

The distal lung contains terminal bronchioles and alveoli that facilitate gas exchange. Three-dimensional *in vitro* human distal lung culture systems would strongly facilitate investigation of pathologies including interstitial lung disease, cancer, and SARS-CoV-2-associated COVID-19 pneumonia. We generated long-term feeder-free, chemically defined culture of distal lung progenitors as organoids derived from single adult human alveolar epithelial type II (AT2) or KRT5$^+$ basal cells. AT2 organoids exhibited AT1 transdifferentiation potential while basal cell organoids developed lumens lined by differentiated club and ciliated cells. Single cell analysis of basal organoid *KRT5*$^+$ cells revealed a distinct *ITGA6*$^+$*ITGB4*$^+$ mitotic population whose proliferation further segregated to a *TNFRSF12A*^{hi} subfraction comprising ~10% of KRT5$^+$ basal cells, residing in clusters within terminal bronchioles and exhibiting enriched clonogenic organoid growth activity. Distal lung organoids were created with apical-out polarity to display ACE2 on the exposed external surface, facilitating SARS-CoV-2 infection of AT2 and basal cultures and identifying club cells as a novel target population. This long-term, feeder-free organoid culture of human distal lung, coupled with single cell analysis, identifies unsuspected basal cell functional heterogeneity and establishes a facile *in vitro* organoid model for human distal lung infections including COVID-19-associated pneumonia.

The distal lung performs essential respiratory functions which can be compromised by inflammatory, neoplastic or infectious disorders such as COVID-19 pneumonia, whose study would be facilitated by robust human *in vitro* models. The identities of human stem cells that regenerate distal lung epithelium *in vivo* over the lifespan are inferred from mouse despite differences between these species[1]. In humans, basal stem cells span the entire airway tree in contrast to mouse where club cells[2] and/or Secretoglobin 1A1 (SCGB1A1)-expressing non-club cells[3] renew the distal bronchioles during aging. In the gas exchange region, murine alveolar epithelial type II (AT2) cells generate AT1 and AT2 cells during homeostasis[4,5], and additional progenitors are recruited by severe injury[3,6–9]. The presence and/or roles of facultative progenitors in human lung is unknown. Human AT2 cells can be differentiated into AT1 cells but cultures are short-lived, neither demonstrating long-term self-renewal nor enabling expansion for disease modeling[4,10,11], while requirements for feeder cells impede definition of specific niche components[12,13]. Here, we established long-term organoid culture of distal human lung, including AT2 and basal stem cells, which was applied to functional progenitor validation and SARS-CoV-2 modeling.

Clonogenic alveolar and basal organoids

We empirically defined media conditions supporting clonal expansion of distal human lung progenitors in collagen/laminin extracellular matrix from 136 individuals (Fig. 1a, Supplementary Table 1).

[1]Division of Hematology, Department of Medicine, Stanford University School of Medicine, Stanford, CA, USA. [2]Division of Infectious Disease and Geographic Medicine, Department of Medicine, Stanford University School of Medicine, Stanford, CA, USA. [3]Stanford University School of Engineering, Department of Electrical Engineering, Stanford, CA, USA. [4]Department of Microbiology and Immunology, Stanford University School of Medicine, Stanford, CA, USA. [5]Stanford ChEM-H and Department of Chemistry, Stanford University, Stanford, CA, USA. [6]Department of Pediatrics, Stanford University School of Medicine, Stanford, CA, USA. [7]10x Genomics Inc., Pleasanton, CA, USA. [8]Department of Epidemiology, University of North Carolina at Chapel Hill, Chapel Hill, NC, USA. [9]Stanford Institute of Immunity, Transplantation and Infection, Stanford University School of Medicine, Stanford, CA, USA. [10]Department of Molecular and Cellular Physiology, Stanford University School of Medicine, Stanford, CA, USA. [11]Division of Biomedical Data Science, Department of Medicine, Stanford University School of Medicine, Stanford, CA, USA. [12]Division of Pulmonary, Allergy and Critical Care, Department of Medicine, Stanford University School of Medicine, Stanford, CA, USA. [13]Division of Gastroenterology, Department of Medicine, Stanford University School of Medicine, Stanford, CA, USA. [14]Department of Biochemistry, Stanford University School of Medicine, Stanford, CA, USA. [15]Howard Hughes Medical Institute, Stanford University School of Medicine, Stanford, CA, USA. [16]Department of Microbiology and Immunology, University of North Carolina at Chapel Hill, Chapel Hill, NC, USA. [17]Chan Zuckerberg Biohub, San Francisco, CA, USA. [18]Present address: Division of Hematology and Oncology, Department of Medicine, University of Illinois at Chicago College of Medicine, Chicago, IL, USA. [19]These authors contributed equally: Ameen A. Salahudeen, Shannon S. Choi. ✉e-mail: cblish@stanford.edu; tdesai@stanford.edu; cjkuo@stanford.edu

Together, EGF and the BMP antagonist NOGGIN supported growth of disaggregated distal lung cells or purified epithelial fractions thereof (Extended Data Fig. 1a-c). Single cells (Extended Data Fig. 1d-g) expanded into either SFTPC$^+$HTII-280$^+$ AT2 cystic organoids (Fig. 1b–e) or KRT5$^+$ solid organoids expressing the basal cell marker KRT5 (Fig. 1b, f–h).

Single cell RNA-sequencing (scRNA-seq) of distal lung organoids confirmed *SFTPC*$^+$ AT2, *KRT5*$^+$ basal and *SCGB1A1*$^+$ club cell populations (Fig. 1i–j, Extended Data Fig. 2). Cells co-expressing *KRT5* and *SCGB1A1* bridged basal and club populations, suggesting a transitional state (Fig. 1j-k, Extended Data Fig. 2) supported by SPADE[14] and Monocle[15] trajectory analysis (Extended Data Fig. 3, Supplementary Table 2).

Human AT2 organoid characterization

We generated pure AT2 organoids from mixed cultures via lamellar body uptake of lysosomal dyes (Extended Data Fig. 4a-b, Supplementary Figure 1). EPCAM$^+$LysoTracker$^+$ AT2 cells clonally expanded up to 180 days (Fig. 1l-m, Extended Data Fig. 4c-d). Chemically defined EGF/NOGGIN medium was sufficient for baseline clonal AT2 organoid proliferation that was attenuated by blocking endogenous WNT biosynthesis (Extended Data Fig. 4e), recapitulating essential autocrine WNT signaling in mouse AT2 cells[16]. Growth was enhanced by adding fibroblast conditioned medium containing serum and Wnt agonists (Extended Data Fig. 4f). Transmission electron microscopy revealed microvilli and lamellar bodies characteristic of mature AT2 cells (Fig. 1n, Extended Data Fig. 4g). AT2 organoids upregulated AT1 markers when cultured on glass with serum (Fig. 1o-p).

Single cell RNA-seq of mixed distal lung organoids or purified alveolar organoids revealed uniformly high-level expression of canonical AT2 cell markers in alveolar populations (Fig. 1i-k, Fig. 1q, Extended Data Fig. 2, Supplementary Data 1). AT2 cell subsets were not readily observed, and cell cycle mRNAs did not localize to a specific AT2 subpopulation (Fig. 1q, Supplementary Data 1, Supplementary Table 3).

Differentiation of human basal organoids

Basal cell organoids in mixed distal lung culture grew more rapidly than alveolar organoids and initially formed solid KRT5$^+$ spheroids (Fig. 1a-b, f-h). However, by 1 month ~50% of organoids developed single or occasionally multiple lumens (Fig. 2a-b, Extended Data Fig. 5a-c) with emergence of club (SCGB1A1$^+$KRT5$^-$) and ciliated (AcTUB$^+$KRT5$^-$) cells lining the interior surface (Fig. 2a, b). Basal cultures purified by density sedimentation exhibited serial clonal outgrowth, EGF and NOGGIN dependence, and cavitation lined by luminal SCGB1A1$^+$ club and AcTUB$^+$ ciliated cells (Extended Data Fig. 5d–h, Fig. 2c-d, Supplementary Video 1-2). Similar differentiation occurred upon organoid transfer to 2D air-liquid interface (ALI) culture (Fig. 2e).

Distinct subtypes of airway basal cells

scRNA-seq clustering of organoid *KRT5*$^+$ basal cells from multiple individuals reproducibly identified two populations, Basal 1 and Basal 2 (Fig. 2f–g, Extended Data Fig. 6a, Supplementary Data 1). Basal 1 included an actively cycling subpopulation (Basal 1.2) enriched in proliferation markers (*PCNA*, *CDK1*) and GSEA cell cycle processes (Fig. 2f-g, Extended Data Fig. 6a-c, Supplementary Table 3). Basal 1 but not Basal 2 expressed canonical lung basal cell mRNAs such as *TP63*[17], integrin α_6 (*ITGA6*) and integrin β_4 (*ITGB4*) encoding a binding partner of ITGA6[18] and marking murine Lineage Negative Epithelial Progenitors (LNEPs)[7] (Fig. 2h). Basal 2 was enriched in vesicular transport, endoplasmic reticulum processes and squamous markers (Fig. 2g, Supplementary Table 3).

TNFRSF12A$^+$ progenitor characterization

We examined the differentially expressed Basal 1 gene *TNFRSF12A* (Fn14, TWEAKR) encoding a membrane receptor (Fig. 2g–h, Supplementary Table 4) given potential utility for FACS isolation and homology to the intestinal stem cell marker *TNFRSF19*[19]. Unbiased pseudotime analysis revealed a continuous single-cell trajectory connecting *KRT5*$^+$ Basal 1 to *SCGB1A1*$^+$ club cells where *TNFRSF12A* mRNA was strongly associated with proliferation marker *MKI67* (Fig 2i, Extended Data Fig. 3). When Basal 1 cells co-expressing *EPCAM*, *ITGA6* and *ITGB4* were divided into *TNFRSF12A*-low, -medium and -high mRNA-expressing fractions, a proliferative gene module[20] was significantly enriched in the highest (*TNFRSF12A^{hi}*) versus lowest quartile (*TNFRSF12A^{lo}*) (Extended Data Fig. 6d-f). To determine if this correlation reflected intrinsic proliferative potential, we fractionated total distal lung organoids by FACS into EPCAM$^+$ITGA6$^+$ITGB4$^+$ Basal 1 cells and then TNFRSF12A^{hi} and TNFRSF12A^{neg} subsets (Fig. 2j), which upon culture revealed 4-12x greater clonogenic organoid-forming capacity of the former (Fig. 2k-l).

We examined lineage relationships between Basal 1 and Basal 2 by fractionating density-sedimented KRT5$^+$ basal organoids by FACS into EPCAM$^+$ITGA6$^+$ITGB4$^+$TNFRSF12A^{hi} (Basal 1) and EPCAM$^+$ITGA6$^-$ITGB4$^-$TNFRSF12A^{neg} (Basal 2) populations (Extended Data Fig. 7a). Clonogenic organoid formation was strongly enriched in Basal 1 versus Basal 2 from three separate individuals (Extended Data Fig. 7b-d). Basal 2-enriched genes *SPRR1B* and *TMSB4X* (Fig. 2g, Supplementary Table 3) were transiently induced in Basal 1 cell organoids (Extended Data Fig. 7e-f), suggesting potential Basal 2 differentiation from Basal 1.

The NOTCH target gene *HES1* was one of the most differentially expressed Basal 1 loci, where gene networks included *NOTCH1*, *NOTCH2* and *JAG1* (Fig. 2g, Supplementary Table 3). NOTCH inhibition significantly increased basal organoid proliferation from TNFRSF12A^{hi}EPCAM$^+$ITGA6$^+$ITGB4$^+$ cells (Extended Data Fig. 7g-h), suggesting NOTCH restraint of growth. Conversely, NOTCH agonism did not affect proliferation but induced *SCGB1A1*, similar to upper airway cells[21,22] (Extended Data Fig. 7i).

TNFRSF12A$^+$ cell characterization in lung

Immunostaining of human distal lung revealed TNFRSF12A$^+$ basal cells enriched intermittently at the tips or bases of bronchiolar furrows (Fig. 3a, Extended Data Fig. 8a-b), the latter recognized as a goblet cell niche[23]. TNFRSF12A was detected in diverse lung stromal and epithelial cells yet clearly marked a minor population of KRT5$^+$ and p63$^+$ basal cells (Fig. 3a, Extended Data Fig. 8a-c). The TNFRSF12A$^+$ subset of KRT5$^+$ basal cells exhibited a higher mitotic index than total KRT5$^+$ cells *in vivo* (Fig. 3b-c), consistent with organoid scRNA-seq (Fig. 2i). FACS analysis of human distal lung confirmed TNFRSF12A expression in 10.9% of basal cells (Extended Data Fig. 8d, top).

Upon prospective culture directly from human lung without an organoid intermediate, FACS-isolated EPCAM$^+$ITGA6$^+$ITGB4$^+$TNFRSF12A^{hi} cells (i.e., TNFRSF12A^{hi} Basal 1) (Extended Data Fig. 8d, **bottom**) exhibited 15-fold increased KRT5$^+$ organoid formation versus EPCAM$^+$ITGA6$^+$ITGB4$^+$TNFRSF12A^{neg} cells (i.e., TNFRSF12^{neg} Basal 1) (Fig. 3d-e). TNFRSF12A^{hi} basal organoids also differentiated to SCGB1A1$^+$ club and AcTUB$^+$ ciliated cells in prolonged culture (Fig. 3f) or when transitioned to 2D ALI (Fig. 3g).

SARS-CoV-2 and H1N1 organoid infection

Influenza virus H1N1 avidly infected distal lung organoids, which also expressed influenza receptors (Extended Data Fig. 9a-d), similar to proximal airway organoids[24,25]. Organoid influenza H1N1 PR8 infection was inhibited by nucleoside analogs consistent with previous studies[26] (Extended Data Fig. 9e), and screening of diverse antiviral compound

classes in 48-well format revealed differential activity (Extended Data Fig. 9f), suggesting utility for scalable therapeutics discovery.

In COVID-19 pneumonia, severe distal lung SARS-CoV-2 infection induces alveolar damage and respiratory failure[27]. Organoid scRNA-seq at time points prior to ciliated differentiation revealed SARS-CoV-2 receptor *ACE2* and processing protease *TMPRSS2* mRNAs predominantly in club and AT2 cells (Extended Data Fig. 10a), consistent with ACE2 expression in KRT5$^-$ differentiated interior luminal cells (Fig. 2a). To facilitate SARS-CoV-2 access to ACE2-expressing luminal cells we adapted an apical-out suspension culture polarization method[28] to distal lung organoids (Extended Data Fig. 10b). Within 48h in suspension, organoids reorganized into apical-out epithelial spheroids with microvilli, apical junctions, and motile cilia facing the organoid exterior. Differentiation of outwardly oriented ciliated cells accelerated over 5 days and progressed over weeks (Fig. 4a; Extended Data Fig. 10c-f; Supplemental Video 3). Apical-out basal organoids also displayed increased outwardly facing club cells with apical secretory granules (Fig. 4a; Extended Data Fig. 10g) while apical-out AT2 organoids exhibited AT1 differentiation (Extended Data Fig. 10h-j). Crucially, in apical-out organoids, ACE2 localized to apical cell membranes on the external organoid surface (Fig. 4b, Extended Data Fig. 10k).

SARS-CoV-2 infected apical-out mixed distal lung organoids with induction of unspliced SARS-CoV-2 genomic RNA to levels approaching the abundantly expressed U3 snoRNA (Fig. 4c, **left**), replication-specific SARS-CoV-2 subgenomic RNA (sgRNA) (Fig. 4c, **right**) and infectious virion production with VeroE6 cell plaque formation (35 PFU/mL from organoid lysates and 65 PFU/mL from organoid supernatants). In SARS-CoV-2-infected basal organoids, double-stranded RNA (dsRNA) appeared by 48h (Fig. 4d) and SARS-CoV-2 nucleocapsid protein (NP) by 96h (Fig. 4e). Approximately 10% of AT2 organoids displayed prominent SARS-CoV-2 NP expression in SFTPC$^+$ cells; remaining organoids were devoid of infection (Fig. 4f). Similarly, SARS-CoV-2 infected ~10% of basal organoids. In 2,621 total distal airway basal cells representing cultures from 4 individuals (Supplementary Table 5), SARS-CoV-2 infection was not detected in KRT5$^+$ basal or AcTUB$^+$ ciliated cells (odds ratio 0, p-value < 0.05), in contrast to SARS-CoV-2 infection of upper airway ciliated cells in 2D ALI culture[29,30]. However, SARS-CoV-2 NP and dsRNA immunofluorescence were primarily present in SCGB1A1$^+$ club cells (Fig. 4g-h) which were strongly associated with and accounted for 79% of NP/dsRNA-positive cells (odds ratio 19.33, p < 0.0001); 21% of infected cells lacked SCGB1A1 (Fig. 4g-h, Supplementary Table 5). Overall, these studies indicated direct SARS-CoV-2 infection of AT2 cells, and implicated club cells as a novel distal lung target population.

Discussion

Here, we applied long-term human distal lung organoid cultures to progenitor discovery and infectious disease modeling. Our findings extend upon prior short-term and feeder-dependent adult lung culture methods[4,10,11] and present an alternative to iPSC differentiation techniques[31–34]. Organoids contained interrelated subtypes of KRT5$^+$ human distal lung basal cells, Basal 1 and Basal 2. Notably, the TNFRSF12A-expressing Basal 1 subfraction possessed enriched clonogenic progenitor activity, establishing functional precedent for a proliferation-enriched basal cell subtype. TNFRSF12A, while by no means exclusively present in basal cells, within the basal layer often localizes to a postulated niche in airway furrow bases and tips[23], extending recent notions of lung epithelial spatial specialization[35]. Conceivably, TNFRSF12A or analogous markers could distinguish basal cell progenitor subsets in other tissues. The current organoids also enable facile exploration of SARS-CoV-2 distal lung infection, relevant to COVID-19-associated pneumonia[27] and implicate SCGB1A1$^+$ club cells as a novel target whose infection could compromise protective lung glycosaminoglycans and precipitate a vicious infection cycle. Ciliated cell infection was not observed, in contrast to 2D ALI lung studies[29,30] and could require alternative culture conditions. SCGB1A1-negative populations were also infected and are under further investigation; for example, bronchial transient secretory cells express *ACE2* and *TMPRSS2*[36].

Overall, single cell analysis of organoid cultures, exemplified here, may represent a general strategy for identifying and functionally validating candidate stem cells in slowly proliferating tissues. The culture of progenitors for all adult distal lung epithelial lineages, including alveoli, should substantially enable disease modeling including neoplastic and interstitial lung conditions[12] and allow tissue engineering and precision medicine applications. Finally, this organoid system should facilitate diverse investigations of pulmonary pathogens, including the SARS-CoV-2 distal lung infection associated with fulminant respiratory failure.

Online content

Any methods, additional references, Nature Research reporting summaries, source data, extended data, supplementary information, acknowledgements, peer review information; details of author contributions and competing interests; and statements of data and code availability are available at https://doi.org/10.1038/s41586-020-3014-1.

1. Hogan, B. & Tata, P.R. Cellular organization and biology of the respiratory system. *Nat Cell Biol* (2019).
2. Rawlins, E.L., *et al*. The role of Scgb1a1+ Clara cells in the long-term maintenance and repair of lung airway, but not alveolar, epithelium. *Cell Stem Cell* **4**, 525-534 (2009).
3. Kathiriya, J.J., Brumwell, A.N., Jackson, J.R., Tang, X. & Chapman, H.A. Distinct Airway Epithelial Stem Cells Hide among Club Cells but Mobilize to Promote Alveolar Regeneration. *Cell Stem Cell* **26**, 346-358.e344 (2020).
4. Barkauskas, C.E., *et al*. Type 2 alveolar cells are stem cells in adult lung. *J Clin Invest* **123**, 3025-3036 (2013).
5. Desai, T.J., Brownfield, D.G. & Krasnow, M.A. Alveolar progenitor and stem cells in lung development, renewal and cancer. *Nature* **507**, 190-194 (2014).
6. Liu, Q., *et al*. Lung regeneration by multipotent stem cells residing at the bronchioalveolar-duct junction. *Nat Genet* **51**, 728-738 (2019).
7. Vaughan, A.E., *et al*. Lineage-negative progenitors mobilize to regenerate lung epithelium after major injury. *Nature* **517**, 621-625 (2015).
8. Zuo, W., *et al*. p63(+)Krt5(+) distal airway stem cells are essential for lung regeneration. *Nature* **517**, 616-620 (2015).
9. Juul, N.H., Stockman, C.A. & Desai, T.J. Niche Cells and Signals that Regulate Lung Alveolar Stem Cells In Vivo. *Cold Spring Harb Perspect Biol* (2020).
10. Sucre, J.M.S., *et al*. Successful Establishment of Primary Type II Alveolar Epithelium with 3D Organotypic Coculture. *Am J Respir Cell Mol Biol* **59**, 158-166 (2018).
11. Zacharias, W.J., *et al*. Regeneration of the lung alveolus by an evolutionarily conserved epithelial progenitor. *Nature* **555**, 251-255 (2018).
12. Nikolic, M.Z. & Rawlins, E.L. Lung Organoids and Their Use To Study Cell-Cell Interaction. *Current pathobiology reports* **5**, 223-231 (2017).
13. Evans, K.V. & Lee, J.H. Alveolar wars: The rise of in vitro models to understand human lung alveolar maintenance, regeneration, and disease. *Stem Cells Transl Med* **9**, 867-881 (2020).
14. Anchang, B., *et al*. Visualization and cellular hierarchy inference of single-cell data using SPADE. *Nat Protoc* **11**, 1264-1279 (2016).
15. Cao, J., *et al*. The single-cell transcriptional landscape of mammalian organogenesis. *Nature* **566**, 496-502 (2019).
16. Nabhan, A., Brownfield, D.G., Harbury, P.B., Krasnow, M.A. & Desai, T.J. Single-cell Wnt signaling niches maintain stemness of alveolar type 2 cells. *Science* (2018).
17. Rock, J.R., *et al*. Basal cells as stem cells of the mouse trachea and human airway epithelium. *Proc Natl Acad Sci U S A* **106**, 12771-12775 (2009).
18. Kajiji, S., Tamura, R.N. & Quaranta, V. A novel integrin (alpha E beta 4) from human epithelial cells suggests a fourth family of integrin adhesion receptors. *EMBO J* **8**, 673-680 (1989).
19. Stange, D.E., *et al*. Differentiated troy(+) chief cells act as reserve stem cells to generate all lineages of the stomach epithelium. *Cell* **155**, 357-368 (2013).
20. Whitfield, M.L., George, L.K., Grant, G.D. & Perou, C.M. Common markers of proliferation. *Nat Rev Cancer* **6**, 99-106 (2006).
21. Rock, J.R., *et al*. Notch-dependent differentiation of adult airway basal stem cells. *Cell Stem Cell* **8**, 639-648 (2011).
22. Pardo-Saganta, A., *et al*. Injury induces direct lineage segregation of functionally distinct airway basal stem/progenitor cell subpopulations. *Cell Stem Cell* **16**, 184-197 (2015).
23. Quinton, P.M. Both Ways at Once: Keeping Small Airways Clean. *Physiology (Bethesda)* **32**, 380-390 (2017).
24. Zhou, J., *et al*. Differentiated human airway organoids to assess infectivity of emerging influenza virus. *Proc Natl Acad Sci U S A* **115**, 6822-6827 (2018).
25. Imai, M. & Kawaoka, Y. The role of receptor binding specificity in interspecies transmission of influenza viruses. *Curr Opin Virol* **2**, 160-167 (2012).

26. Kumaki, Y., Day, C.W., Smee, D.F., Morrey, J.D. & Barnard, D.L. In vitro and in vivo efficacy of fluorodeoxycytidine analogs against highly pathogenic avian influenza H5N1, seasonal, and pandemic H1N1 virus infections. *Antiviral research* **92**, 329-340 (2011).
27. Zhu, N., *et al*. A Novel Coronavirus from Patients with Pneumonia in China, 2019. *N Engl J Med* **382**, 727-733 (2020).
28. Co, J.Y., *et al*. Controlling Epithelial Polarity: A Human Enteroid Model for Host-Pathogen Interactions. *Cell Rep* **26**, 2509-2520.e2504 (2019).
29. Lamers, M.M., *et al*. SARS-CoV-2 productively infects human gut enterocytes. *Science* **369**, 50-54 (2020).
30. Hou, Y.J., *et al*. SARS-CoV-2 Reverse Genetics Reveals a Variable Infection Gradient in the Respiratory Tract. *Cell* **182**, 429-446.e414 (2020).
31. Dye, B.R., *et al*. In vitro generation of human pluripotent stem cell derived lung organoids. *Elife* **4** (2015).
32. Chen, Y.W., *et al*. A three-dimensional model of human lung development and disease from pluripotent stem cells. *Nat Cell Biol* **19**, 542-549 (2017).
33. Jacob, A., *et al*. Differentiation of Human Pluripotent Stem Cells into Functional Lung Alveolar Epithelial Cells. *Cell Stem Cell* **21**, 472-488.e410 (2017).
34. Yamamoto, Y., Korogi, Y., Hirai, T. & Gotoh, S. A method of generating alveolar organoids using human pluripotent stem cells. *Methods in cell biology* **159**, 115-141 (2020).
35. Montoro, D.T., *et al*. A revised airway epithelial hierarchy includes CFTR-expressing ionocytes. *Nature* **560**, 319-324 (2018).
36. Lukassen, S., *et al*. SARS-CoV-2 receptor ACE2 and TMPRSS2 are primarily expressed in bronchial transient secretory cells. *EMBO J* **39**, e105114 (2020).

Publisher's note Springer Nature remains neutral with regard to jurisdictional claims in published maps and institutional affiliations.

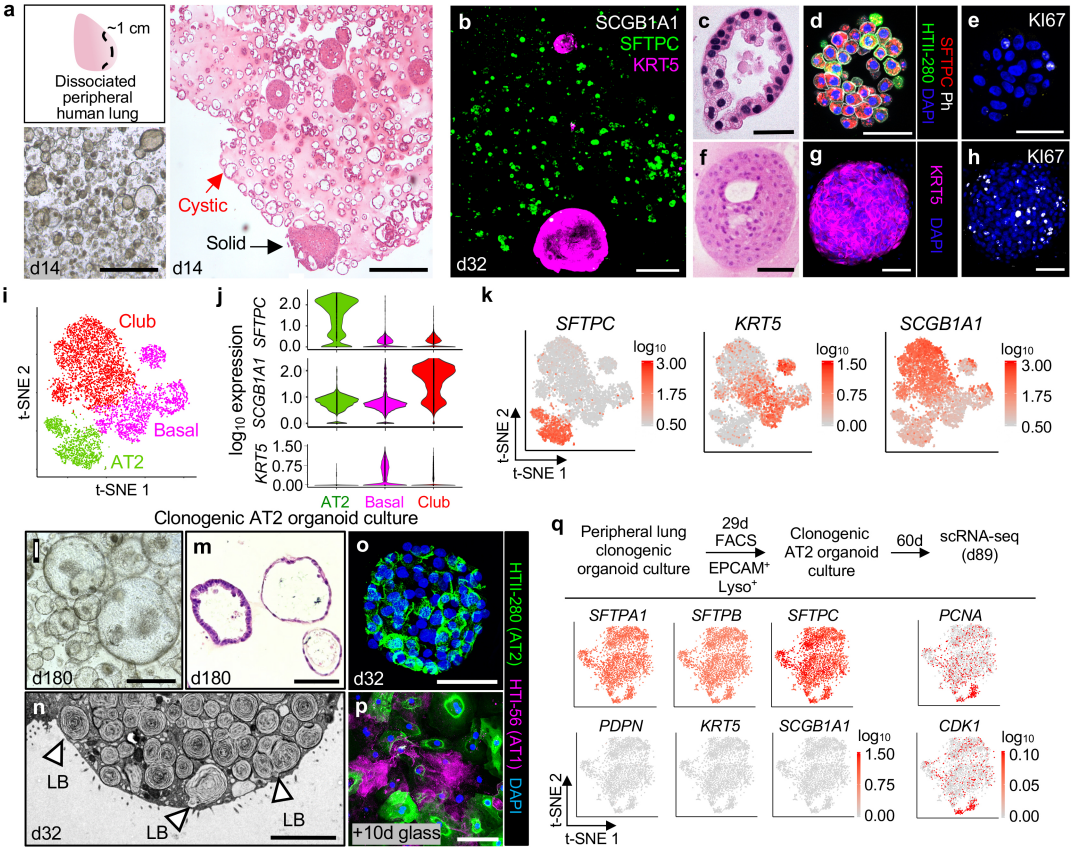

Fig. 1 | Clonogenic expansion of human distal lung organoids. a. Human distal lung d14 (day 14) organoid cultures contain cystic and solid organoids, brightfield and H&E. Scale bar 100 µm. **b**, Whole-mount immunofluorescence (IF), anti-KRT5 (basal), -SFTPC (AT2) and -SCGB1A1 (club), scale bar 100 µm, d32. **c-e**, Alveolar organoids, d32. **c**, Cystic AT2 organoid, H&E, scale bar 25 µm. **d**, Whole-mount fluorescence for anti-SFTPC, anti-HTII-28, phalloidin and DAPI, scale bar 50 µm. **e**, Anti-Ki67 and DAPI of adjacent section of (d). **f-h**, Basal organoids, d32. **f**, H&E, scale bar 50 µm. **g**, Whole-mount IF, anti-KRT5 and DAPI, scale bar 100 µm. **h**, Anti-Ki67 and DAPI immunostaining of (g). **i-k**, scRNA-seq of d28 total distal lung organoids. **i**, t-SNE plot of 7,285 individual cells demonstrating AT2, basal, and club populations. **j**, Violin plot, *SFTPC* (AT2), *KRT5* (basal), *SCGB1A1* (club). **k**, Feature plots, tSNE. **l**, Brightfield microscopy, AT2 organoids d180, scale bar 200 µm. **m**, H&E from (l), d180, scale bar 50 µm. **n**, Transmission electron microscopy of d32 AT2 organoid, LB = lamellar body, scale bar 5 µm. **o-p**, AT2 organoid at d32 (o); culture on glass for 10 additional days induces AT1 differentiation (p). Anti-HTI-56 (AT1) and -HTII-280 (AT2) IF staining, scale bar 50 µm. **q**, scRNA-seq feature plots of 2,780 AT2 organoid cells, day 89 cumulative culture.

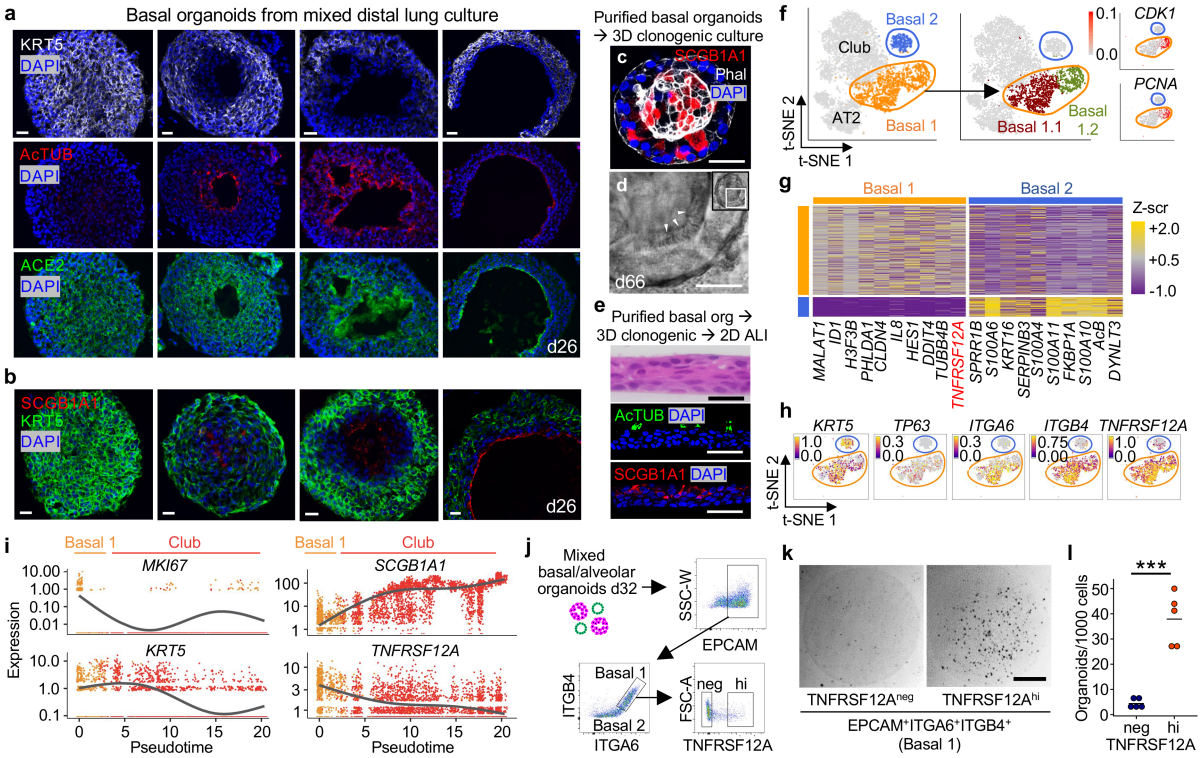

Fig. 2 | Basal organoid differentiation and TNFRSF12A^{hi} progenitor discovery. a-b, Basal organoid differentiation in mixed culture. Lumens are lined by acetylated tubulin^{+} (AcTUB) ciliated (a) and SCGB1A1^{+} club cells (b) which express SARS-CoV-2 receptor ACE2 but lack KRT5, IF, d26, scale bar 20 µm. **c-e**, Sedimented basal organoid culture. **c**, Club differentiation, d38, shown by whole-mount fluorescence for anti-SCGB1A1 (red), phalloidin (white), and DAPI (blue), scale bar 50 µm. **d**, Ciliated differentiation, confocal transmission image, scale bar 20 µm. **e**, AcTUB^{+} ciliated and SCGB1A1^{+} club cells upon organoid replating in 2D ALI, IF, scale bar 50 µm. **f-g**, scRNA-seq of *KRT5*$^{+}$ basal cells from Fig. 1i. **f**, Basal 1 and Basal 2 subclusters. Basal 1 is subdivided into Basal 1.1 and 1.2, the latter expressing proliferative mRNAs *CDK1* and *PCNA*, tSNE. **g**, Basal 1 and Basal 2 differential gene expression. **h**, Basal marker transcript t-SNE overlays of (f), $\log_{10}$ UMI. **i**, Relative gene expression kinetic plots of (f-g) across the pseudotime trajectory ($n = 3,721$ cells). **j**, FACS isolation of TNFRSF12A^{hi} versus TNFRSF12A^{neg} cells from mixed distal lung organoids, pre-gated on live singlets. **k**, d14 organoid culture of (j), brightfield. **l**, Quantitation of (k), *** = $p < 0.001$ ($p = 1.0 \times 10^{-4}$) two-tailed Student's t-test. Data in j-k represent n = 5 independent experiments for each TNFRSF12A population.

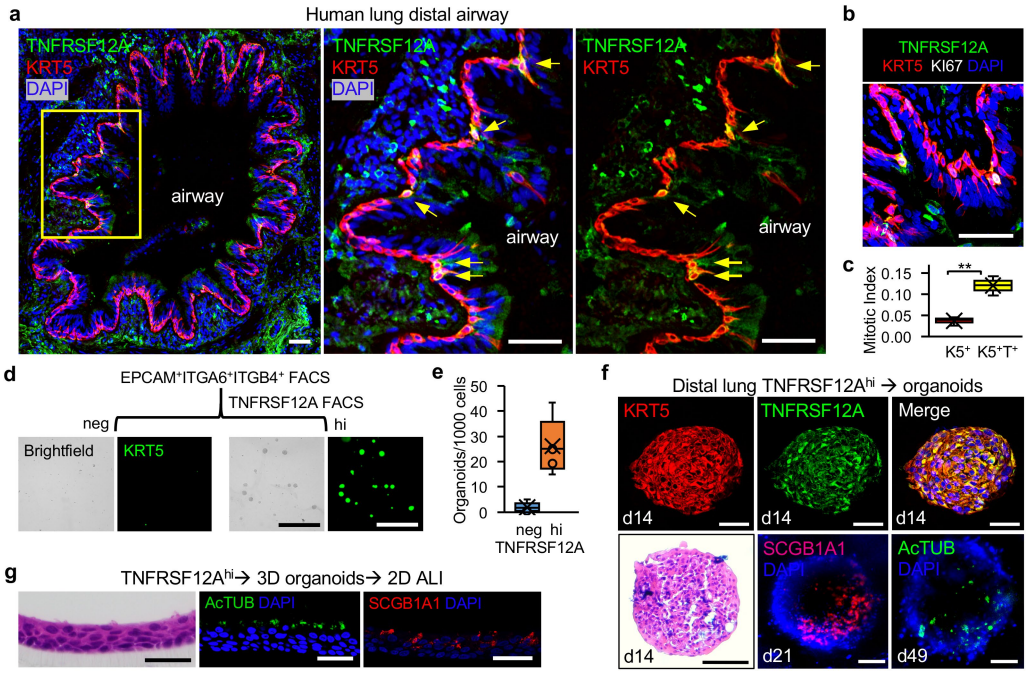

Fig. 3 | Characterization of TNFRSF12A^{hi} Basal 1 cells from intact human lung. a, Left, anti-KRT5 (red) and anti-TNFRSF12A (green) IF of human distal lung, DAPI = blue, scale bar 100 µm. The left panel yellow boxed area is depicted with (middle) and without (right) DAPI, scale bar 100 µm. **b**, Distal airway TNFRSF12A^{+} basal cell proliferation, IF, KRT5 (red), TNFRSF12A (green), KI67 (white), DAPI (blue). Scale bar 100 µm. **c**, Mitotic index of TNFRSF12A^{+} KRT5^{+} cells from (b), 3 independent experiments. K5^{+} = total KRT5^{+}, K5^{+}T^{+} = TNFRSF12A^{+} KRT5^{+}, boxplots represent first quartile, median, third quartile, and whiskers represent minimum and maximum ** = $p < 0.01$ (4.4×10^{-3}), two tailed student's t-test. **d**, Anti-KRT5 IF of FACS-isolated TNFRSF12A^{neg} and TNFRSF12A^{hi} d14 organoid culture, scale bar 500 µm. **e**, Quantitation of (d); Data in d represent n = 5 independent experiments for each TNFRSF12A population. Boxplots represent first quartile, median, third quartile, and whiskers represent minimum and maximum, $p = 1.1 \times 10^{-3}$, two tailed student's t-test. **f**, H&E and anti-KRT5, -TNFRSF12A, -SCGB1A1, and -AcTUB immunostaining of organoids from the TNFRSF12A^{hi} fraction of FACS-sorted EPCAM^{+}ITGA6^{+}ITGB4^{+} distal lung. Scale bar 50 µm. **g**, H&E and anti-SCGB1A1 or AcTUB IF of 2D ALI cultures from basal cell organoids from TNFRSF12A^{hi} basal cells as in (f). Scale bar 50 µm.

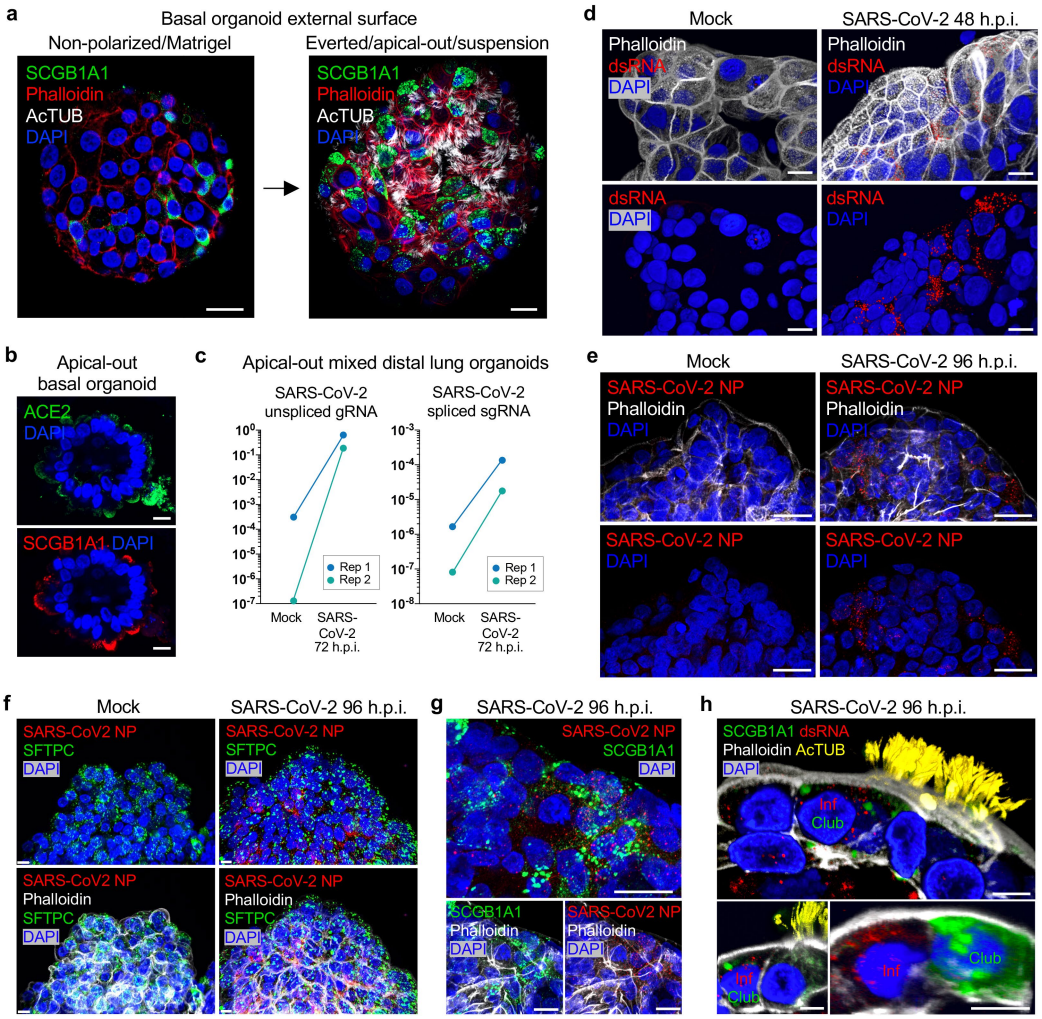

Fig. 4 | SARS-CoV-2 infection of apical-out distal lung organoids. **a**, Polarization and surface localization of SCGB1A1$^+$ club cells (green) and AcTUB$^+$ ciliated cells (white) upon ECM non-polarized growth (left) or apical-out suspension culture (right), IF. **b**, Transverse section of apical-out basal organoid as in (a), stained with anti-ACE2 (green), -SCGB1A1 (red), and DAPI (blue). **c**, SARS-CoV-2 unspliced genomic RNA (left) and spliced subgenomic RNA (right) in apical-out distal lung organoids, 72h post-infection (h.p.i.), qPCR, n = 2 independent experiments. **d**, Anti-double-stranded RNA (dsRNA) IF, apical-out human distal lung organoids, mock vs. SARS-CoV-2, 48 h.p.i. **e**, SARS-CoV-2 nucleocapsid protein (NP) IF, apical-out organoids, mock vs. 96 h.p.i. **f**, SARS-CoV-2-infected apical-out AT2 organoids, IF with the indicated antibodies, 96 h.p.i. **g**, IF colocalization of SARS-CoV-2 NP and SCGB1A1, apical-out distal lung basal organoids, 96 h.p.i. **h**, SARS-CoV-2 infection cell type specificity in apical-out organoids, IF with the indicated antibodies. Inf = SARS-CoV-2 infected cell. In **c**-**h**, organoids were in suspension for 6-10 days (basal) and 3 days (AT2) prior to infection. All scale bars 20 µm except for f, h (10 µm).

Methods

Additional experimental details are in the Supplementary Methods.

Human tissue procurement and processing

All experiments performed in this work was approved by the Stanford University School of Medicine Institutional Review Board and performed under protocol #28908. Standard informed consent for research was obtained in writing from all patients who contributed to this study prior to tissue procurement and all experiments followed relevant guidelines and regulations. Peripheral lung tissue within 1 cm of the visceral pleura was obtained from surgical discards from lobectomies. For patients with suspected lung cancer, cases with clinical T4 (American Joint Cancer Committee 6th edition) disease (e.g. features such as bronchial invasion or parenchymal satellite nodule/ metastases) were deferred. Normal tissue was harvested from the lung margin most anatomically distal to palpably well-defined lesions, or from uninvolved lobes in the case of pneumonectomies. Samples with tumors containing ill-defined margins were deferred. Tissue was either processed fresh or placed at 4 °C overnight and processed the following morning.

Mixed distal lung organoid culture

To isolate distal airway cells, lung parenchyma 1 cm from the visceral pleura was mechanically dissociated with Castro scissors, washed and incubated with 5 units/ml porcine elastase (Worthington), 100 Kunitz Units/mL DNase I (Worthington), and Normocin (InvivoGen), and resuspended in two tissue volumes of lung organoid media, comprised of Advanced DMEM/F12 (Invitrogen) supplemented with 10 mM nicotinamide, n-acetyl cysteine, 1X B27 supplement minus vitamin A, recombinant human NOGGIN (100 ng/mL, R&D Systems), recombinant human EGF (50 ng/mL, R&D Systems), and TGF-beta inhibitor A83-01 (100 nM, Tocris). This lung organoid medium was used for all experiments except for Extended Data Fig. 4f. The tissue was then agitated for one hour at 37 °C and the resultant cell suspension was filtered through 100 through 40 µm cell strainers and subjected to ammonium chloride red blood cell lysis. The cell pellet was then washed and resuspended in 10 volumes of reduced growth factor Basement Membrane Extract II (Trevigen). Cells in matrix were then plated in 24-well plates in 50 microliter droplets, and warm media was added after the droplets solidified for ten minutes at room temperature Media was changed every 3-4 days and organoids were passaged every 3-4 weeks by dissociation with TrypLE. Passaging was based on ECM durability/integrity and estimated organoid confluency, judged by estimated organoid volume to volume of the ECM droplet. Distal lung organoids could be passaged for ~6 months with basal organoids initially exhibiting 6-7 doublings every 2 weeks. Alveolar organoids expanded more slowly with an initial rate of 3-4 doublings/2 weeks but predominated over basal organoids after several months. Based on initial cell division rates, the upper limits of basal and alveolar expansion were 2^{19} (524,288 fold) and 2^{16} (65,536 fold) respectively. To rule out contamination by malignant cells, long-term cultures were systematically evaluated for the presence of dysplasia or carcinoma by a board-certified pathologist. In addition, five long-term organoid cultures (2-6 months) underwent targeted Next Generation Sequencing to exclude pathogenic nucleotide variants (see below). Full details are provided in Supplementary Methods.

Tandem MACS stromal depletion and EPCAM purification of distal lung cells

Distal lung was dissociated as above, and all incubation steps were carried out on ice. 10^7 cells were incubated with Fc Block (Biolegend 422301) and diluted 1:100 in FACS buffer (2 mM EDTA and 0.2% fetal calf serum in 1X PBS pH 7.4), for ten minutes followed by APC-conjugated anti-CD45 antibodies at 1 µg/mL in FACS buffer for 30 minutes, washed, and subjected to two rounds of depletion with magnetic beads according to manufacturer's protocol (Miltenyi: anti-human fibroblast 130-050-601, anti-CD31130-091-935, anti-APC 130-090-855, LS column 130-042-401). Unlabeled cells were then centrifuged at 300 x *g* and labeled with a cocktail of 1 µg/mL of PerCP-Cy5.5 anti-EPCAM antibody and Zombie Aqua viability stain (Biolegend 423101) diluted 1:400 from stock concentration in FACS buffer.

Organoid Cryopreservation and Recovery

For cryopreservation and recovery, ECM droplets were dissociated by pipetting in 3 volumes of PBS + 5 mM EDTA and then incubated on ice for one hour. Cells were pelleted at 300 x *g* for 5 minutes and resuspended in freezing medium (fetal calf serum (Gibco), 10% v/v DMSO), placed into cryovials and then into Mr. Frosty™ (Thermo Fisher) containers and stored in a -80C freezer overnight, followed by transfer to liquid nitrogen vapor phase for long term storage. Organoids were recovered by quick thaw in a 37 °C water bath followed by washing in organoid media and plating in ECM with organoid media plus 10 µM ROCK inhibitor Y-27632 (Tocris).

Screening exogenous growth factors in organoid culture

Distal airway cells were isolated and plated as above with the following exceptions: Advanced DMEM/F12 was used instead of organoid medium during elastase digestion of lung tissue, cells were serially diluted and filtered through a 40 micron cell strainer and counted with a hemocytometer. 1000 viable epithelial cells (by Trypan blue exclusion, size, and morphology) per µl ECM were plated per 5 µl Matrigel droplet per well. Base media consisted of organoid media lacking A83-01, EGF, NOGGIN, WNT3A or RSPO1. EGF (final 50 ng/mL, R&D), NOGGIN (final 100 ng/mL, R&D), WNT3A (final 100 ng/mL, R&D), RSPO1 (final 500 ng/mL, Peprotech) or the PORCUPINE inhibitor C59 (final 1 µM, Biogems) were added singly or in combination to base media. Images were obtained ten days after primary plating with an inverted light microscope at 5X magnification. Each condition was plated in quadruplicate and organoid formation was quantified using the analyze particle (threshold = 490^2 pixels) plugin in ImageJ as previously described[65].

Single Cell RNA-seq of unfractionated organoid cultures

Lung organoid cultures from separate individuals were dissociated 4 weeks after primary plating and subjected to droplet based scRNA-seq with the 10x Genomics Single Cell 3' platform with a 5 nucleotide UMI according to manufacturer's protocol. Cell capture, library preparation, and sequencing were performed as previously described[37]. For scRNA-seq analysis in Fig. 1k, a modified Kruskal-Wallis Rank Sum Test was performed to determine significance of differential marker gene expression for AT2 (*SFTPC*), basal (*KRT5*), and club (*SCGB1A1*), with all p-values < 0.001. Principle Component Analysis, t distributed Stochastic Neighborhood Embedding, unsupervised Graph based clustering, statistical testing, pseudotime trajectory for all scRNA-seq analyses are described in Supplementary Methods and Supplementary Data 1.

Single cell RNA-seq of purified AT2 organoid cultures

LysoTracker$^+$ AT2 cells[38] from unfractionated organoids were purified by FACS and cultured for two months with one passage. These were dissociated and subjected to droplet-based scRNA-seq with the 10x Genomics Chromium Single Cell 3' platform v2 according to the manufacturer's protocol. The library was sequenced using paired-end sequencing (26bp Read 1 and 98bp Read 2) with a single sample index (8bp) on an Illumina NextSeq 500. Data preprocessing and Principle Component Analysis were carried out with CellRanger v1.2. Subsequent analysis is described in Supplementary Methods and Supplementary Data 1.

Electron microscopy

Organoid cultures were fixed in ECM with 2.5% glutaraldehyde in 0.1 M cacodylate buffer (pH 7.4), dehydrated, embedded in epoxy resin and visualized with a JEOL (model JEM1400) transmission-electron microscope with a LaB6 emitter at 120 kV.

Histology and immunocytochemistry

Organoids were fixed with 2% paraformaldehyde at 4 °C overnight, paraffin embedded and sectioned (10-20 µm) as previously described[37]. Sections were deparaffinized and stained with H&E for histological analysis. Antibodies used for immunocytochemistry staining are listed in Supplementary Methods following standard staining protocols[39] and images acquired on a Leica-SP8 confocal microscope.

RNA fluorescent in situ hybridization

RNA in situ hybridization was performed according to Nagendran et al.[40] and probe sequences are provided in Supplementary Methods.

Whole-mount organoid confocal immunofluorescence microscopy

Intact, uninfected organoids were fixed in 2% paraformaldehyde in 100 mM phosphate buffer (pH 7.4) (4% paraformaldehyde for infected organoids) for one hour at room temperature, washed with PBS with 100mM glycine, permeabilized 0.5% Triton X-100 in PBS for 1 h, then incubated in staining buffer (4% BSA, 0.05% Tween-20 in PBS pH 7.4, 10% goat/donkey serum) for an additional hour, followed by incubation with primary antibody for 24 h at room temperature in staining buffer. Whole mounts were then washed with PBS-T and incubated with fluorescent secondary antibodies, phalloidin and DAPI, for four hours at room temperature in staining buffer. Following additional washes, whole mounts were submerged in mounting media (VECTASHIELD, Vector Laboratories) and mounted on chambered coverslips for imaging in four channels using Zeiss LSM 700 or 900 confocal microscopes. 3D rendering of confocal image stacks was performed using Volocity Image Analysis software (Quorum Technologies Inc., Guelph, Ontario). For Figure 5j, requiring 5 colors, cilia were distinguished by staining with two fluorescent secondary antibodies and merging the colocalized voxels into a pseudocolored channel using Volocity software. Lectin staining (FITC-Sambuca Nigrin, Vector Labs FL-1301; Biotin-Maackia Amurensis, Vector Labs FL-1301) was carried out according to manufacturer's protocol after fixation of organoids with 0.1% paraformaldehyde in PBS for 1 hour at room temperature followed by blocking with Avidin/Biotin (Vector Labs SP-2001). Biotin-Maackia Amurensis lectin was labeled with streptavidin-PE conjugate (Thermo Fisher SA10041) and after washing lectin staining was imaged in a Keyence BZ-X700.

Next generation sequencing of organoid cultures

Ten organoid cultures were sequenced using a commercial targeted resequencing assay with end-to-end coverage of 131 cancer genes and companion software (TOMA COMPASS Tumor Mutational Profiling System, Foster City, CA) to determine the presence of oncogenic mutations in long-term organoid cultures. Libraries were sequenced on an Illumina NextSeq 500. Nonsynonymous variants are listed in Supplementary Table 6. Variant Call Files are provided in Supplementary Data 2.

Density sedimentation of basal cells

Organoid cultures within 2-3 weeks of primary plating were dissociated with 1 U/mL neutral protease (Worthington, Cat LS02100) and 100 KU of DNase I in lung organoid media. Basal organoids were then collected by gravity sedimentation and the supernatant was either aspirated or collected for downstream use. Basal organoids were then further fractionated on a custom Ficoll-Paque gradient (4 vol Ficoll-Paque to 1 vol PBS) and centrifuged at 300 x *g* for 10 minutes at room temperature. Supernatant was aspirated and the organoid pellet resuspended in 10 ml PBS in a 15 mL conical tube, collected by gravity sedimentation, and plated into ECM as described above.

FACS isolation and culture of AT2 cells

Organoids were dissociated with TrypLE followed by neutralization with 10% volume fetal calf serum, subjected to DNase at 100 kU/mL, washed with lung organoid media and then incubated with 100 cell pellet volumes of lung organoid media with 10 nM LysoTracker Red DND-99 (Thermo Fisher L7528) at 37 °C for 30 minutes. Cells were then washed and resuspended in FACS buffer as described above, incubated with Fc block, followed by incubation on ice with labeling cocktail consisting of 1 µg/mL of PerCP-Cy5.5 anti-EPCAM antibody and Zombie Aqua viability stain (Biolegend 423101) diluted 1:400 from stock concentration in FACS buffer. EPCAM^{hi} and LysoTracker^{hi} cells were sorted into lung organoid media + 10 µM Y-27632 (Tocris 1254) and cultured in ECM and lung organoid media with Y-27632 for 24 hours, followed by lung organoid media without Y-27632. Pure AT2 organoid growth was enhanced by addition of 1:1 vol:vol serum-containing L-cell conditioned media (L-WRN CM) containing WNT3A, R-SPONDIN3 and NOGGIN and supplemented with recombinant EGF[41]. Full gating strategy is provided in Supplementary Figure 1. All FACS antibodies were purchased from Biolegend. Qualitatively identical results could also be obtained with anti-HTII-280 (AT2 marker, Terrace Biotech) FACS purification in lieu of LysoTracker. AT2 organoid cells were transdifferentiated to AT1 cells by TrypLE dissociation from ECM and seeding onto chambered glass coverslips followed by culturing with Advanced DMEM/F12 + 5% fetal calf serum[42].

Color mixing studies with lentivirally transduced GFP and mCherry

FACS EPCAM^{+} stromal-depleted organoids at d14 were infected with lentivirus at an estimated MOI of 0.9 according to Van Lidth de Jeude et al.[43] with third generation lentiviral vectors (PGK-GFP T2A Puro, SBI cat# CD550A-1; mCherry modified from pLentiCRISPRv1 (Addgene #49545) to incorporate an EF-1a-mCherry P2A Puro cassette, a gift from Paul Rack). 96 hours after infection, organoids were treated with puromycin at a concentration of 600 ng/mL for 48 hours to select for transduced cells. Two weeks after selection, GFP-expressing organoids or mCherry-expressing organoids were dissociated to single cells and mixed in a 1:1 ratio and scored as monochromatic or mixed after 28 days of each passage. The same approach was employed for purified AT2 and basal cultures after respective purification strategies from an initial FACS EPCAM^{+} stromal depleted organoid starter culture.

Flow cytometry analysis of resident basal cells from adult human lung

Adult human lung tissue was procured and dissociated as above but cells were labeled with Zombie Aqua live:dead stain as above, washed with FACS buffer, and then fixed in 2% PFA in PBS overnight at 4 °C . Cells were then stained using the whole mount procedure as described above with the omission of PBS glycine washing. Fixed and permeabilized cells were then incubated with 1:400 dilution of Alexa Fluor 647 conjugated mouse anti-human cytokeratin 5 antibody (Abcam) for 24 hours at 4 °C in permeabilization buffer. Cells were then washed with FACS buffer and labeled with PE conjugated mouse anti-human TNFRSF12A antibody (clone ITEM-4, Biolegend) for 30 minutes on ice, followed by washing and analysis on a BD Aria Fusion instrument. Full gating strategy and qPCR validation of ITEM-4 antibody is detailed in Supplementary Figure 1.

FACS isolation of TNFRSF12A^{hi} and TNFRSF12A^{neg} basal cells

Single cell suspensions from either fresh human distal lung or primary organoid culture at approximately 4 weeks of culture were dissociated as above, treated with Fc Block (BioLegend), and incubated in FACS buffer with Zombie Aqua 1:400, 1 µg/mL PerCP-Cy5.5 anti-human EpCAM (CD326), 1 ug/mL APC anti-human ITGA6 (CD49f), 2 ug/mL FITC anti-human ITGB4 (CD104), and 1 µg/mL PE anti-human TNFRSF12A (CD266). 30 minutes after labeling the cells were washed twice with FACS buffer and sorted for EPCAM^{hi}, ITGA6/ITGB4^{hi}, TNFRSF12A^{hi} and TNFRSF12A^{neg}. Full gating strategy is provided in Supplementary Figure 1. > 5000 cells were sorted into Eppendorf tubes with lung

organoid medium and 10 µM ROCK inhibitor Y-27632. All FACS antibodies were purchased from Biolegend.

Culture of TNFRSF12A^{hi} and TNFRSF12A^{neg} basal cells

Cells were seeded in ECM and submerged in lung organoid media with 10 µM ROCK inhibitor Y-27632. Seeding density for cells FACS isolated from organoid culture was 1000 cells per well at a density of 100 cells/µl of ECM. Seeding for cells FACS isolated from fresh human distal lung was 3000 cells per well at a density of 300 cells/µl of ECM. After 24 hours, the media was changed to remove ROCK inhibitor and additionally changed every 72 hours. Organoid formation was manually quantified 14 days post plating by two independent observers.

H1N1 organoid influenza assay

Unfractionated cultures containing AT2, basal, and club cell types at 2-3 weeks were infected in triplicate with PR8 strain of H1N1 modified to express GFP upon viral replication[44] after 24 hours of pretreatment with antiviral compounds. ECM was dispersed by addition of 5 mM EDTA in PBS, followed by washing and inoculation with PR8-H1N1-GFP reporter virus at an estimated MOI of 1 in media containing either vehicle or antivirals. After 12 hours (one influenza infection cycle), intact organoid GFP expression was visualized by either fluorescence microscopy with a Keyence BZ-X700 automated microscope, or dissociated to single cell, fixed with 0.1% PFA in PBS followed by FACS quantitation of GFP$^+$ cells (Gating Strategy is provided in Supplementary Figure 1). Antiviral dose response curves were generated using four-parameter nonlinear regression curve fitting with GraphPad Prism 7 (GraphPad Software, San Diego, CA). H1N1 tropism was assessed in a manner similar to above with the exception of Ficoll sedimented basal cell fraction versus non-basal fractions were dissociated to single cells, counted, and infected with an estimated MOI of 1 in organoid media for one hour at 37 °C, followed by washing and reseeding into ECM, cultured for 16 hours, followed by dissociation and FACS as above.

Suspension culture to generate apical-out polarity in lung organoids

Lung organoids grown embedded in 50 µl ECM droplets were transferred to suspension culture as described[28] with modifications. Briefly, ECM-embedded organoids were dislodged gently by pipetting using sterile LoBind tips (Eppendorf 22493008) and placed in 15 ml LoBind conical tubes (Eppendorf 30122216) containing ice-cold 5 mM EDTA in PBS. 5 ml of EDTA solution was used per ECM-droplet (3 ECM droplets/15 ml conical) rotating 1 h at 4 °C on a rotating platform. Organoids were centrifuged at 200 x g for 3 min at 4 °C and the supernatant was removed. The pellet was re-suspended in growth media in ultra-low attachment 6-well tissue culture plates (Corning Costar 3471). Suspended organoids were incubated at 37 °C with 5% CO_2 for different times (range 0-30 days) to characterize apical-out polarity, ciliogenesis, differentiation, and to prepare apical-out organoids for infection experiments with SARS-CoV-2.

SARS-CoV2 infection of human distal lung organoids

VeroE6 cells were obtained from ATCC and maintained in supplemented DMEM with 10% FBS. SARS-CoV-2 (USA-WA1/2020) was passaged in VeroE6 cells in DMEM with 2% FBS. Titers were determined by plaque assay on VeroE6 cells using Avicel (FMC Biopolymer) and crystal violet (Sigma), viral genome sequence was verified, and all infections were performed with passage 3 virus. Organoids were counted and passaged into suspension media for 6-8 days and then resuspended in virus media or an equal volume of mock media, at a MOI of 1 relative to total organoid cells in the sample, and then incubated at 37 °C under 5% CO_2 for 2 hours. Organoids were then plated in suspension in lung organoid media (apical-out organoids). At the indicated timepoints, organoids were washed lung organoid media and PBS and either resuspended in TRIzol LS (Thermo Fisher), freshly-made 4% PFA in PBS, or 250 µl lung organoid media. Cells resuspended in lung organoid media were lysed by freezing at -80 °C. Culture supernatants were preserved in TRIzol LS or added directly to plaque assay monolayers. All SARS-CoV-2 work was performed in a class II biosafety cabinet under BSL3 conditions at Stanford University.

qPCR analysis of SARS-CoV-2 RNA

RNA from SARS-CoV-2-infected organoids was extracted by adding 750 µl TRIzol (Thermo Fisher Scientific), incubating at 55 °C for 5 min and then adding 150 µl chloroform. After mixing each sample by vortexing for 7 s, the samples were incubated at 25 °C for 5 min and then centrifuged at 12,000 r.p.m. for 15 min at 4 °C. The aqueous layer was carefully removed from each sample, mixed with two volumes of 100% ethanol and purified using an RNA Clean & Concentrator-25 kit (Zymo Research) as per manufacturer instructions. All RNA samples were treated with DNase (Turbo DNA-free kit, Thermo Fisher Scientific). The Brilliant II SYBR Green QRT-PCR 1-Step Master Mix (VWR) was used to convert RNA to cDNA and amplify specific RNA regions on the CFX96 Touch real-time PCR detection system (Bio-Rad). RT reaction was performed for 30 min at 50 °C, 10 min at 95 °C, followed by two-step qPCR with 95 °C for 10 seconds and 55 °C for 30 seconds, for a total of 40 cycles. Two primer sets were used, either to amplify non-spliced SARS-CoV-2 genomic RNA (gRNA) spanning nucleotide positions 14221-14306, or spliced SARS-CoV-2 sgRNA[30]. Primer sequences are in Supplementary Table 7.

TNFRSF12A immunostaining of intact distal lung

Optimal staining of human distal lung tissue was achieved from specimens fixed within 30 minutes of primary surgical resections in 4% paraformaldehyde in PBS. Specimens were incubated in fixative overnight at 4 °C, transferred to 30% sucrose, and embedded into OCT. 10 µm thick frozen sections were cut, subjected to citrate based antigen retrieval (Vector labs) at 70 °C for 30 minutes, followed by blocking for one hour with 10% goat serum in IF wash buffer as described above. Mouse anti-TNFRSF12A (clone ITEM-4, Biolegend) was utilized for Fig. 3a and polyclonal rabbit anti-TNFRSF12A (ThermoFisher PA5-20275) was used for Fig. 3b, f and Extended Data Fig. 8[45]

Live-imaging and confocal microscopy of immobilized apical-out lung organoids

Live organoids were held between two coverslips in a viewing chamber (Lab-Tek II two-chambered coverglass) and filmed using a Nikon TE2000E microscope using differential interference contrast (DIC) microscopy with a 63X objective. Samples were kept at 37 °C with 5% CO_2 during imaging. Digital videos were collected by a Hamamatsu high-resolution ORCA-285 digital camera and rendered using OpenLab 5.5.2 software (Improvision). After recording, samples were fixed and stained without removal from the chambers and transferred to the confocal microscope for immunofluorescence microscopy.

Statistics and reproducibility

Unless stated otherwise, all data are representative of at least two independent experiments with each independent experiment carried out using an organoid culture derived from a unique individual. Box plot bounds span first through third quartiles, horizontal lines represent median values, and whiskers represent data range minima or maxima or in the case of outliers, 1.5 times the interquartile range with outliers represented by data points. t-tests were two-tailed and p values are denoted as * = < 0.05, ** = < 0.01, and *** = < 0.001. Full details are provided in Supplementary Methods.

Reporting summary

Further information on research design is available in the Nature Research Reporting Summary linked to this paper.

Data availability

scRNA-seq datasets have been deposited in Gene Expression Omnibus (https://www.ncbi.nlm.nih.gov/geo/query/acc.cgi?acc=GSE106850) with the accession code GSE106850. Source data are provided with this paper.

Code availability

Scripts to perform analyses of scRNA-seq data are provided with this paper. Custom code is available on GitHub (https://github.com/ameen-salahudeen/lung_organoid).

37. Yan, K.S., *et al*. Non-equivalence of Wnt and R-spondin ligands during Lgr5(+) intestinal stem-cell self-renewal. *Nature* **545**, 238-242 (2017).
38. Van der Velden, J.L., Bertoncello, I. & McQualter, J.L. LysoTracker is a marker of differentiated alveolar type II cells. *Respir Res* **14**, 123 (2013).
39. Chang, J., *et al*. Gpr124 is essential for blood-brain barrier integrity in central nervous system disease. *Nat Med* **23**, 450-460 (2017).
40. Nagendran, M., Riordan, D.P., Harbury, P.B. & Desai, T.J. Automated cell type classification in intact tissues by single-cell molecular profiling. *Elife* **7** (2018).
41. Neal, J.T., *et al*. Organoid Modeling of the Tumor Immune Microenvironment. *Cell* **175**, 1972-1988 e1916 (2018).
42. Dobbs, L.G., Williams, M.C. & Brandt, A.E. Changes in biochemical characteristics and pattern of lectin binding of alveolar type II cells with time in culture. *Biochim Biophys Acta* **846**, 155-166 (1985).
43. Van Lidth de Jeude, J.F., Vermeulen, J.L., Montenegro-Miranda, P.S., Van den Brink, G.R. & Heijmans, J. A protocol for lentiviral transduction and downstream analysis of intestinal organoids. *J Vis Exp* (2015).
44. Manicassamy, B., *et al*. Analysis of in vivo dynamics of influenza virus infection in mice using a GFP reporter virus. *Proc Natl Acad Sci U S A* **107**, 11531-11536 (2010).
45. Karaca, G., *et al*. TWEAK/Fn14 signaling is required for liver regeneration after partial hepatectomy in mice. *PLoS One* **9**, e83987 (2014).

Acknowledgements We thank Kuo and Desai lab members for discussions, the Stanford Tissue Bank, Joseph Shrager, Mark Berry and Winston Trope for tissue acquisition, and the Stanford Stem Cell FACS Facility, Pauline Chu, Aaron McCormick, Daniel Mendoza and Francisco de la Vega and James Zengel for technical expertise. SARS-Related Coronavirus 2, Isolate USA-WA1/2020, NR-52281 was deposited by the CDC and obtained through BEI Resources, NIAID, NIH. Fellowships supporting authors are as follows: A.A.S. - A.P. Giannini, ECOG-ACRIN, Paul Carbone, Stanford Cancer Institute; S.S.C. - Stanford Medical Scientist Training Program; J.Z. - Stanford Graduate Fellowship.; S.M.D. - CIRM Bridges. Funding support is as follows: A.R. - NIH grant T32 AI007502-23; R.A.F. - Damon Runyon Cancer Research Foundation (DRG-2286-17), V.V.U. - Netherlands Organization for Scientific Research Rubicon grant (452181214); C.S. and J.Z. - NSF DMS 1712800 and the Stanford Discovery Innovation Fund; K.C.G. and M.M.D. - HHMI; C.A.B - Burroughs Wellcome Fund Investigators in the Pathogenesis of Infectious Disease Grant 1016687. This work was also supported by CIRM DISC2-09637 to C.J.K. and T.J.D., Bill and Melinda Gates Foundation OPP1113682 to C.J.K., M.A.R, and C.A.B., Novo Nordisk Foundation Challenge Grant to M.R.A and M.M.-C., Mathers Foundation Covid Fund to K.C.G., and NIH grants K08DE027730 to A.A.S, U19AI057229 to M.M.D., R56AI111460 to J.S.G., 5R01HL14254902 to T.J.D., DK11572802 to C.J.K. and K.C.G. and U19AI116484, U01DK085527, U01CA217851, U01CA176299 and U01DE025188 to C.J.K., C.A.B is the Tashia and John Morgridge Faculty Scholar and Chan Zuckerberg Biohub Investigator. T.J.D is the Woods Family Endowed Faculty Scholar in Pediatric Translational Medicine. C.J.K. is the Maureen Lyles D'Ambrogio Professor of Medicine.

Author contributions A.A.S. and S.S.C. conceived, designed, and performed experiments, analyzed data, and wrote the manuscript. A.R. designed and performed SARS-CoV-2 infections, J.Z., V.V.U. and C.S. designed and interpreted single cell RNA-seq studies and R.A.F. performed qRT-PCR. M.M.-C., S.M.D., A.J.M.S, T.U, J.J. and A.B. performed organoid culture and analysis. L.E.W. and M.M.D. designed FACS panels. V.L. and K.C.G. contributed the DLL4 E12 mutant. B.A. and S.P. performed SPADE analysis. K.N. and J.S.G. designed and executed influenza studies. G.X.Y.Z., J.M.T., P.B., S.B.Z. and T.S.M. designed and executed single-cell RNA-seq experiments. C.E.E and R.S.B. advised SARS-CoV-2 studies. P.H. provided in situ hybridization protocols. M.R.A., C.A.B., T.J.D. and C.J.K. conceived and designed experiments, analyzed data, and wrote the manuscript.

Competing interests C.J.K., A.A.S., S.S.C., C.A.B., A.R., M.A.R., M.M-C., S.M.O., T.U. are listed as inventors on provisional patent 63/053,079 describing the methods in this paper. C.J.K. is a founder of Surrozen Inc. All other authors declare no competing interests.

Additional information

Supplementary information is available for this paper at https://doi.org/10.1038/s41586-020-3014-1.

Correspondence and requests for materials should be addressed to C.A.B., T.J.D. or C.J.K.

Peer review information *Nature* thanks the anonymous reviewers for their contribution to the peer review of this work.

Reprints and permissions information is available at http://www.nature.com/reprints.

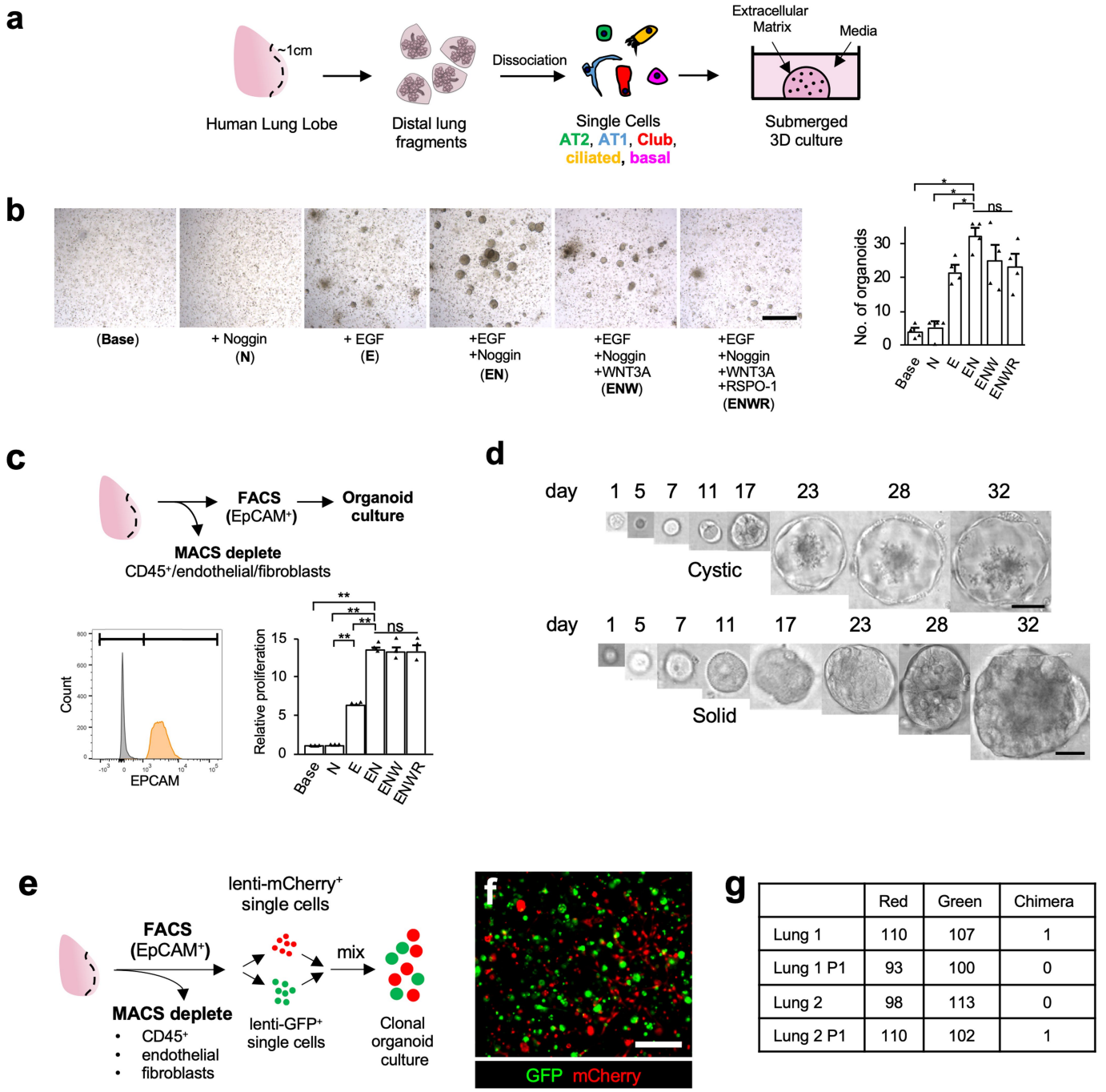

	Red	Green	Chimera
Lung 1	110	107	1
Lung 1 P1	93	100	0
Lung 2	98	113	0
Lung 2 P1	110	102	1

Extended Data Fig. 1 | Optimization of human distal lung organoid culture. **a**, Schematic of culture initiation from human distal lung. **b**, Brightfield microscopy evaluation of required exogenous growth factors and automated organoid quantitation after day 10 of chemically defined organoid culture with specified recombinant growth factors, N=Noggin, E=EGF, W=WNT3A, R=RSPO1, n = 4 per condition, data are mean +/-SEM, *= $p < 0.05$, two-tailed student's t-test, scale bar = 500 µm. **c**, Left, purification schema to isolate epithelial cells from distal human lung involving negative MACS bead depletion of CD45+ hematopoietic cells, endothelial cells and fibroblasts, followed by positive FACS selection for EPCAM+ epithelium. Bottom left, representative FACS demonstrating > 99.9% EPCAM+ purity (orange) upon re-analysis versus unstained controls (grey). Bottom right, proliferation of EPCAM+ cells purified from distal lung cultures after day 10 of organoid culture with specified growth factors, N=Noggin, E=EGF, W=WNT3A, R=RSPO1, n = 3 per condition, data are mean +/- SEM, ** = $p < 0.01$, two-tailed student's t-test. **d**, Time lapse transmission confocal images of solid and cystic organoids originating from single dissociated human distal lung cells, scale bar = 100 µm. **e-g**, Clonality mixing studies. **e**, Schema of mixing studies of lentivirus-GFP- and lentivirus-mCherry-expressing cells to determine clonality. **f**, Representative live fluorescent imaging of resultant green and red organoids from (e), scale bar = 500 µm. **g**, Quantitation of red, green, or chimeric, distal lung organoid cultures from two individuals (1, 2) after initial and serial passaging (P1=passage 1).

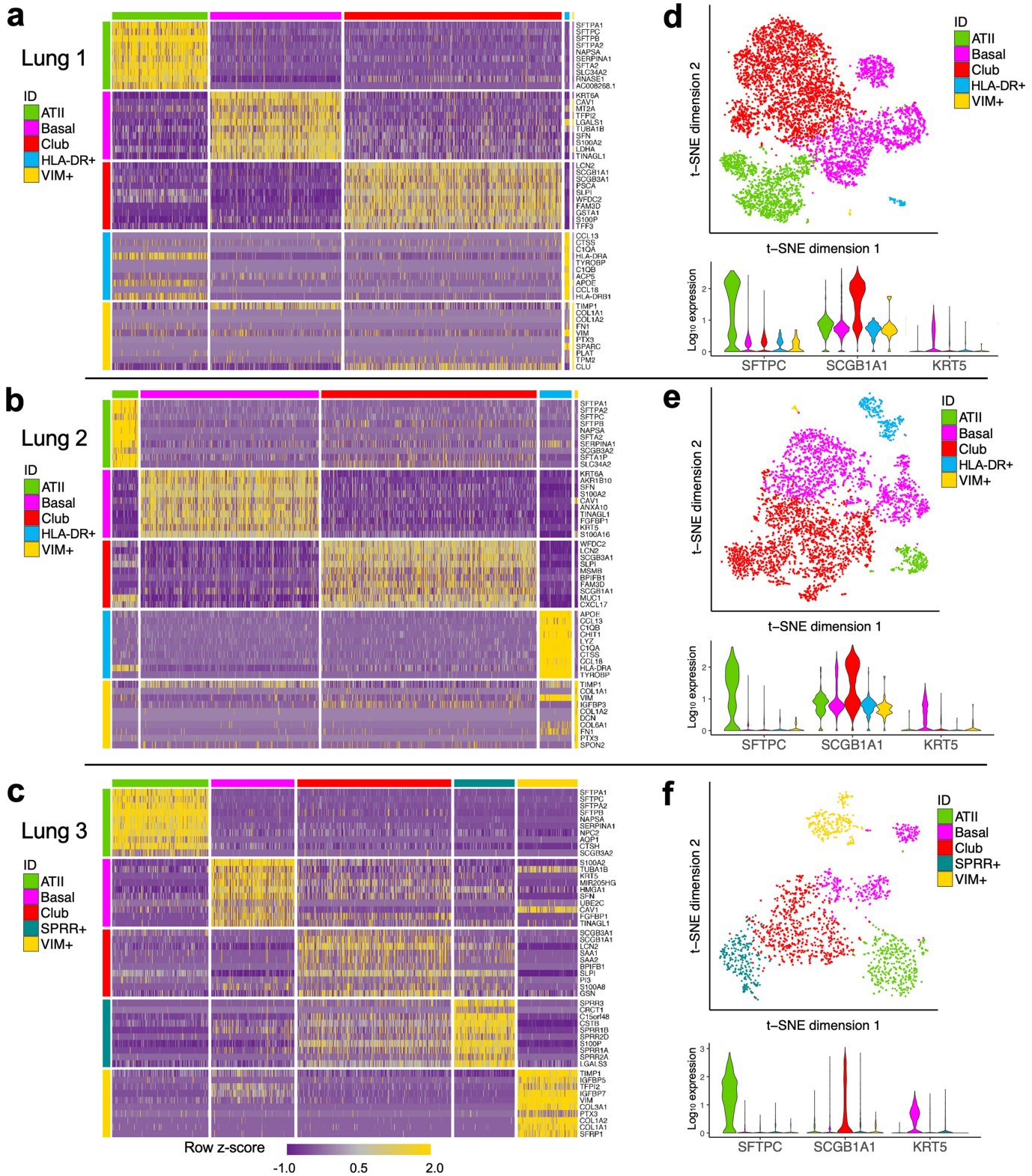

Extended Data Fig. 2 | scRNA-seq of human distal lung organoids cultured from three individuals reveals reproducible basal, club, and AT2 populations. a-c, unsupervised clustering of total cell populations demonstrates consistency in top differentially expressed genes corresponding to basal (*KRT5/6*), club (*SCGB1A1*), and AT2 (*SFTPC*) cells. The epithelial fraction from these cultures ranged from approximately 90-99% of all cells with the remainder being either fibroblasts (*VIM*$^{+}$) or mononuclear cells (HLA-DR+, likely alveolar macrophages). **d-f**, t-SNE visualization and violin plots for marker genes corresponding to each population. Note, a unique population enriched for SPRR genes, which have been described as marker in squamous metaplasia, were exclusively found in the organoid culture of Lung 3, derived from an individual who was an active smoker.

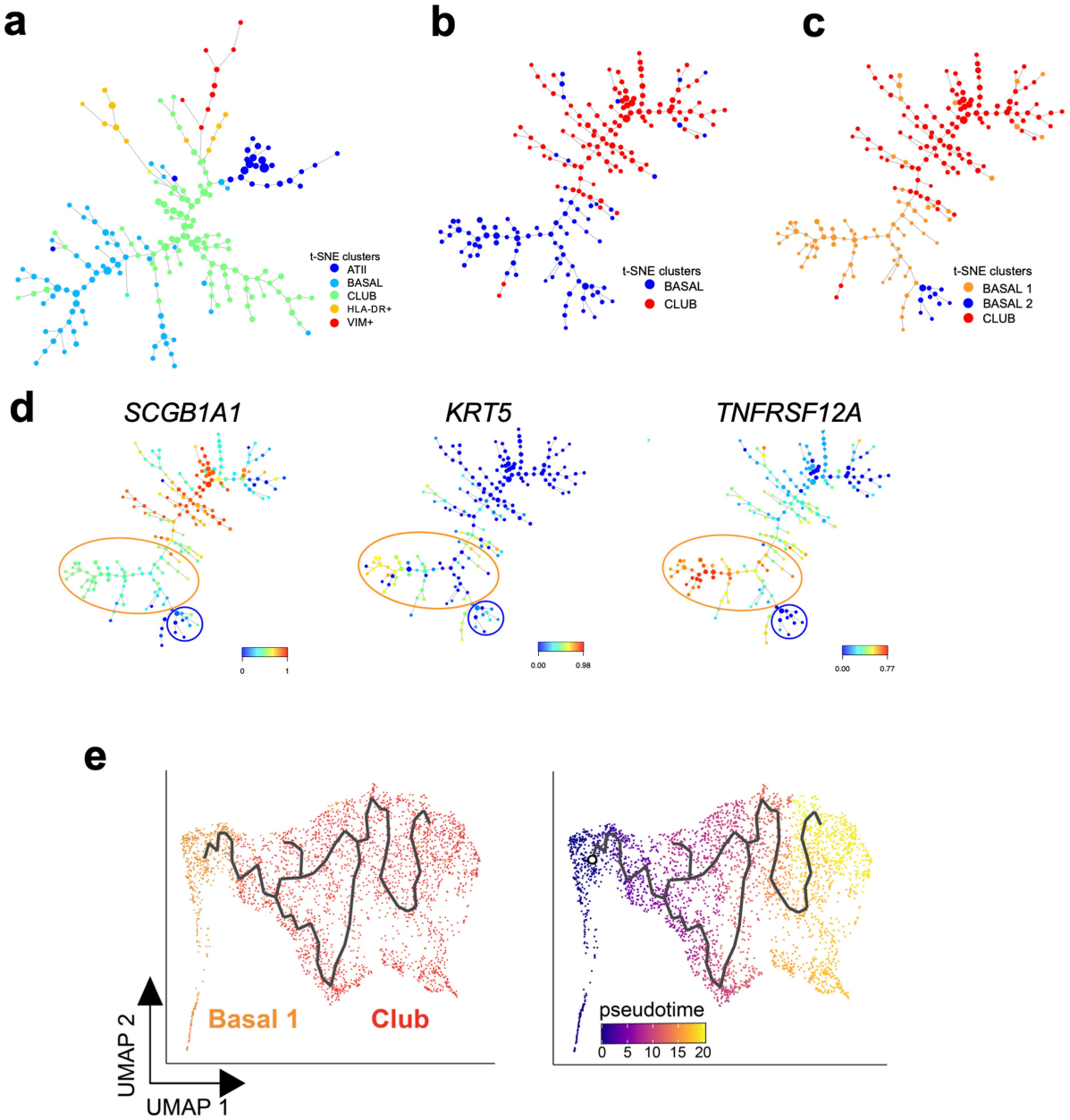

Extended Data Fig. 3 | Trajectory inference with SPADE and pseudotime. **a**, SPADE plot of pooled cells where each point represents cell states that are more related on the same or adjacent branches of a minimum spanning tree. Note: AT2 cells exist on a branch distal to basal and club cells, suggesting no lineage hierarchy between AT2, basal, and club cells. **b**, SPADE plots of pooled scRNA-seq samples after excluding AT2, *VIM*$^{+}$ and *HLA-DR*$^{+}$ cells support lineage relationships between basal (blue) and club (red) populations by club cell branches emanating from basal cells. **c**, SPADE plots of Basal 1, Basal 2, and club populations. **d**, Left, gene expression of SCGB1A1 shows higher expression in club versus basal cell lineages (left) as compared to KRT5 (middle). Right, median gene expression of TNFRSF12A, showing a high (orange outline) and a low (blue outline) within basal cell branches and inferring a potential lineage relationship. **e**, Monocle 3 pseudotime trajectory analysis of single-cell transcriptomes of Basal 1 connected to club cells depicted with UMAP (cell number, $n = 3{,}721$), colored by (left) cell cluster and (right) pseudotime gradient.

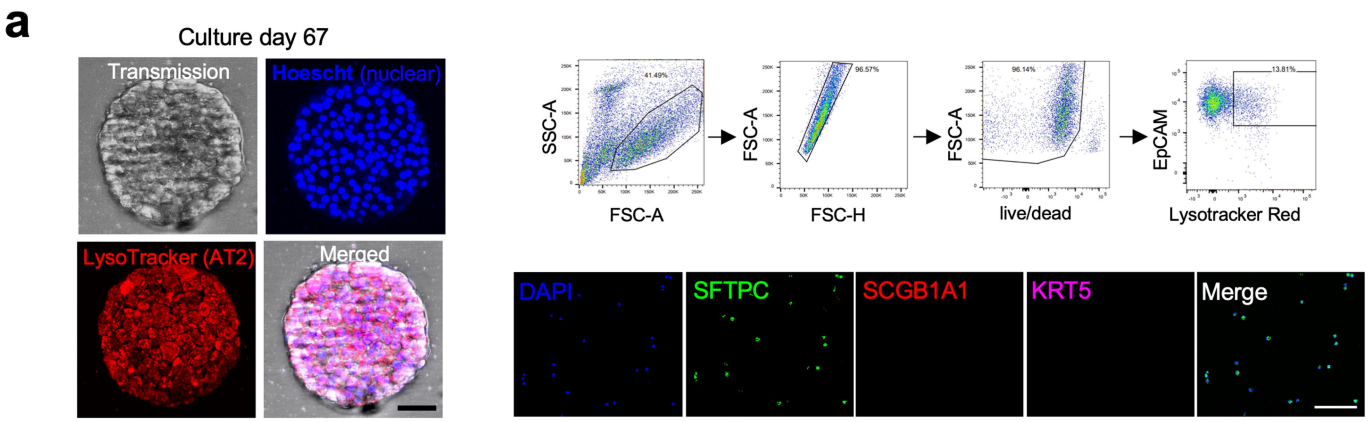

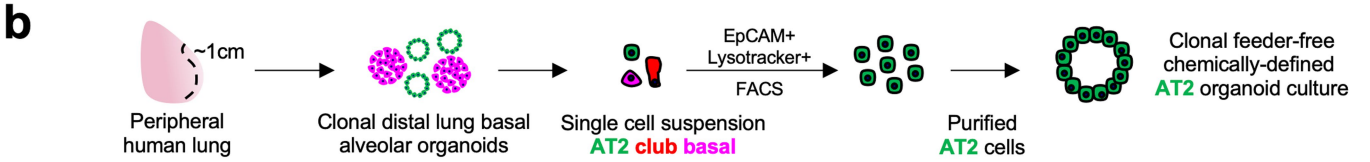

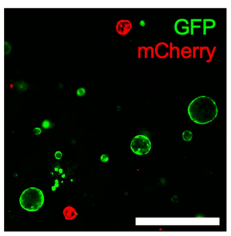

d

	Red	Green	Chimera
Lung 1 P0	67	98	0
Lung 1 P1	89	113	0
Lung 2 P0	74	155	0
Lung 2 P1	80	121	0

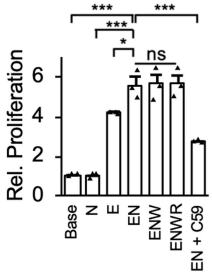

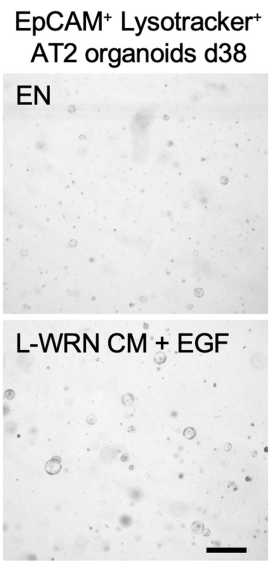

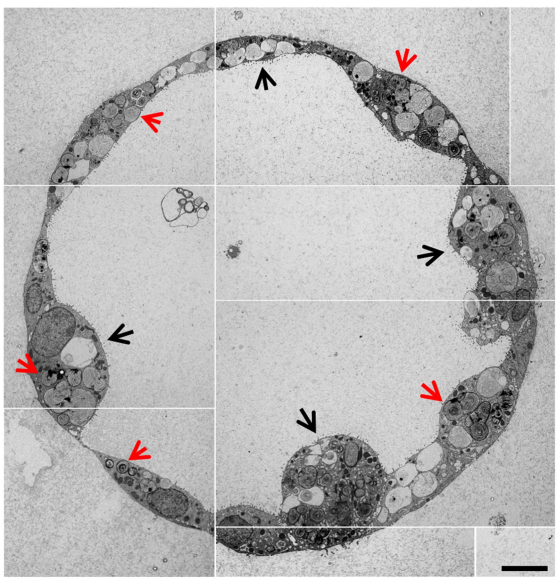

Extended Data Fig. 4 | Human AT2 organoid characterization. a, Left, confocal images of a live AT2 organoid at 67 days of culture labeled with Hoescht nuclear stain and LysoTracker Red DND-99. Top right, isolation of purified AT2 organoids. Representative FACS plots showing LysoTracker Red AT2 purification from unfractionated organoid cultures. Bottom right, immunostaining of cytospin of LysoTracker-sorted AT2 cells show high purity (100/100 cells SPC^+ $SCGB1A1^-$ KRT5); scale bar = 50 µm). **b**, Schema of FACS isolation of AT2 cells from human mixed distal lung organoids as $EPCAM^+LysoTracker^+$ AT2 cells followed by long-term clonogenic organoid culture. **c**, Representative image of clonal mixing studies from stroma-depleted, $EPCAM^+LysoTracker^+$, lentivirally-marked AT2 cells demonstrating presence of completely $mCherry^+$ or GFP^+ but not chimeric organoids carried out as in Extended Data Fig. 1e-g, passage 1 after lentiviral infection, scale bar = 200 µm. **d**, Quantitation of red, green, or chimeric, AT2 organoid cultures as in (c) from two individuals (1, 2) after initial and serial passaging (P1=passage 1). **e**, AT2 organoid proliferation with differing combinations of recombinant niche factors and PORCUPINE inhibitor C59 (1 mM), NOGGIN (N), EGF (E), WNT3A (W), R-SPONDIN1 (R). n = 3 per condition, data are mean +/- SEM, * = $p < 0.05$, *** = $p < 0.001$, two-tailed student's t-test. **f**, Brightfield microscopy comparing pure AT2 organoid growth enhancement in chemically defined lung organoid media (EN) versus serum-containing L-cell conditioned media containing WNT3A, NOGGIN, and R-SPONDIN3 (L-WRN CM) supplemented with recombinant EGF, 1 independent experiment. Scale bar = 200 µm. **g**, Transmission electron microscopy image of representative AT2 organoid at 28 days of culture. Note apical microvilli (black arrows) and lamellar bodies (red arrows); scale bar = 10 µm.

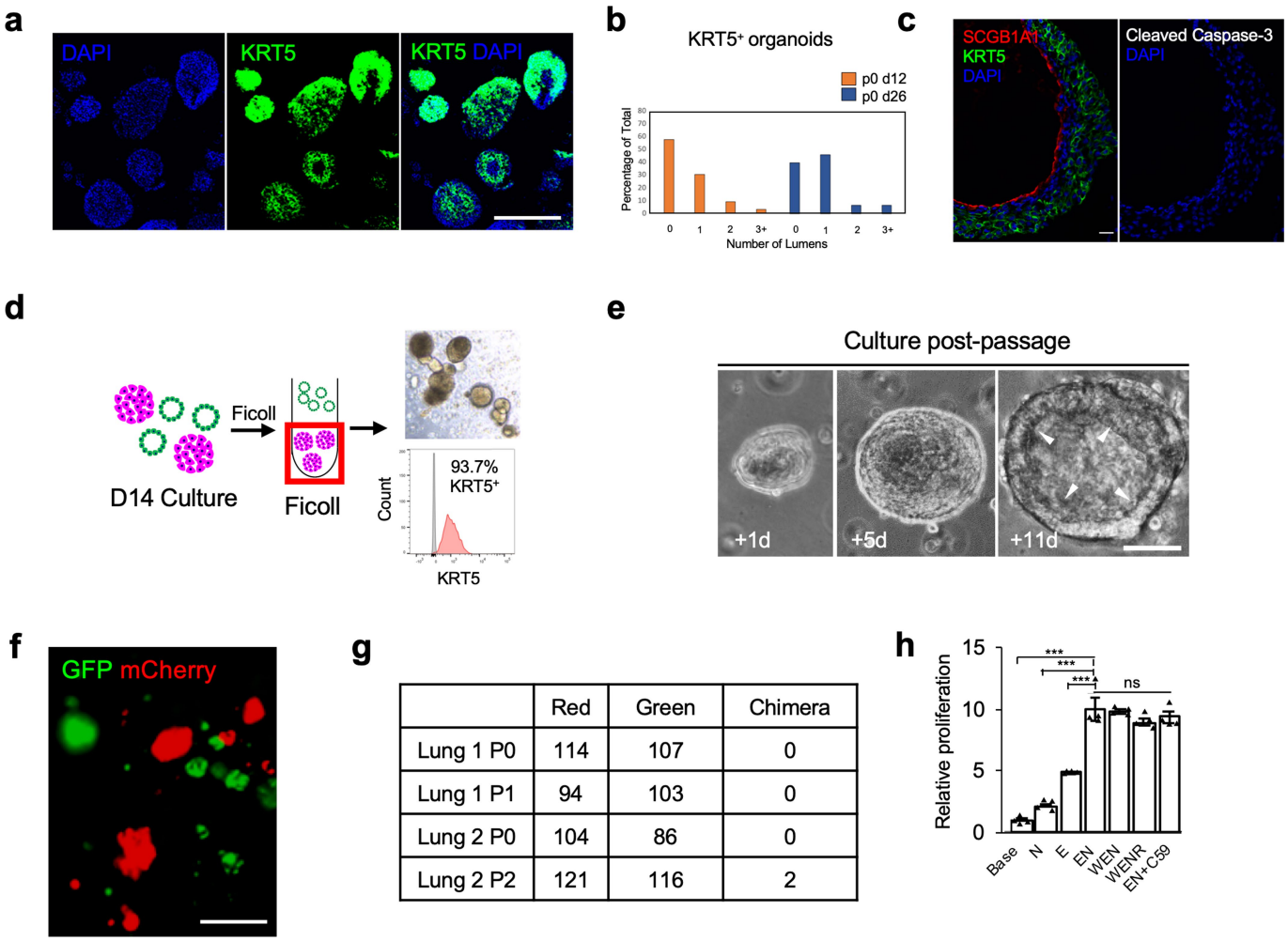

	Red	Green	Chimera
Lung 1 P0	114	107	0
Lung 1 P1	94	103	0
Lung 2 P0	104	86	0
Lung 2 P2	121	116	2

Extended Data Fig. 5 | a-c, Basal organoids in mixed culture progressively form internal lumens, which is not associated with apoptosis. a, KRT5 IF, day 26 culture, scale bar = 200 µm. **b**. Lumen quantitation, d12 versus d26 culture, single determination. **c**, Absence of apoptosis in d26 basal cell organoid internal lumen, cleaved caspase IF, from Fig. 2b, scale bar = 20 µm. **d-e**, Isolation of purified basal cell organoids via differential sedimentation in Ficoll. **d**, Schema and enrichment to > 90% KRT5⁺ cells as measured by intracellular KRT5 FACS of sedimented basal organoid cells; scale bar = 100 µm. **e**, Serial time lapse microscopy of sedimented basal organoids reveals spontaneous cavitation within two weeks post passage or within four weeks of culture initiation; scale bar = 25 µm. **f-g**, Clonal mixing studies from stroma-depleted, Ficoll-purified and lentivirally-marked basal organoid cells demonstrating fully mCherry⁺ or GFP⁺ but not chimeric organoids as in Extended Data Fig. 1f, passage 1 after lentiviral infection, scale bar = 200 µm. **f**, Representative clonal mixing image study. **g**, Quantitation. **h**, Growth factor evaluation for basal organoids after d14 sedimentation, enzymatic dissociation and clonogenic culture. Growth was not affected by the PORCUPINE inhibitor C59 (1 µM). n = 4 per condition, data are mean +/- SEM, *** = $p < 0.001$, two-tailed student's t-test.

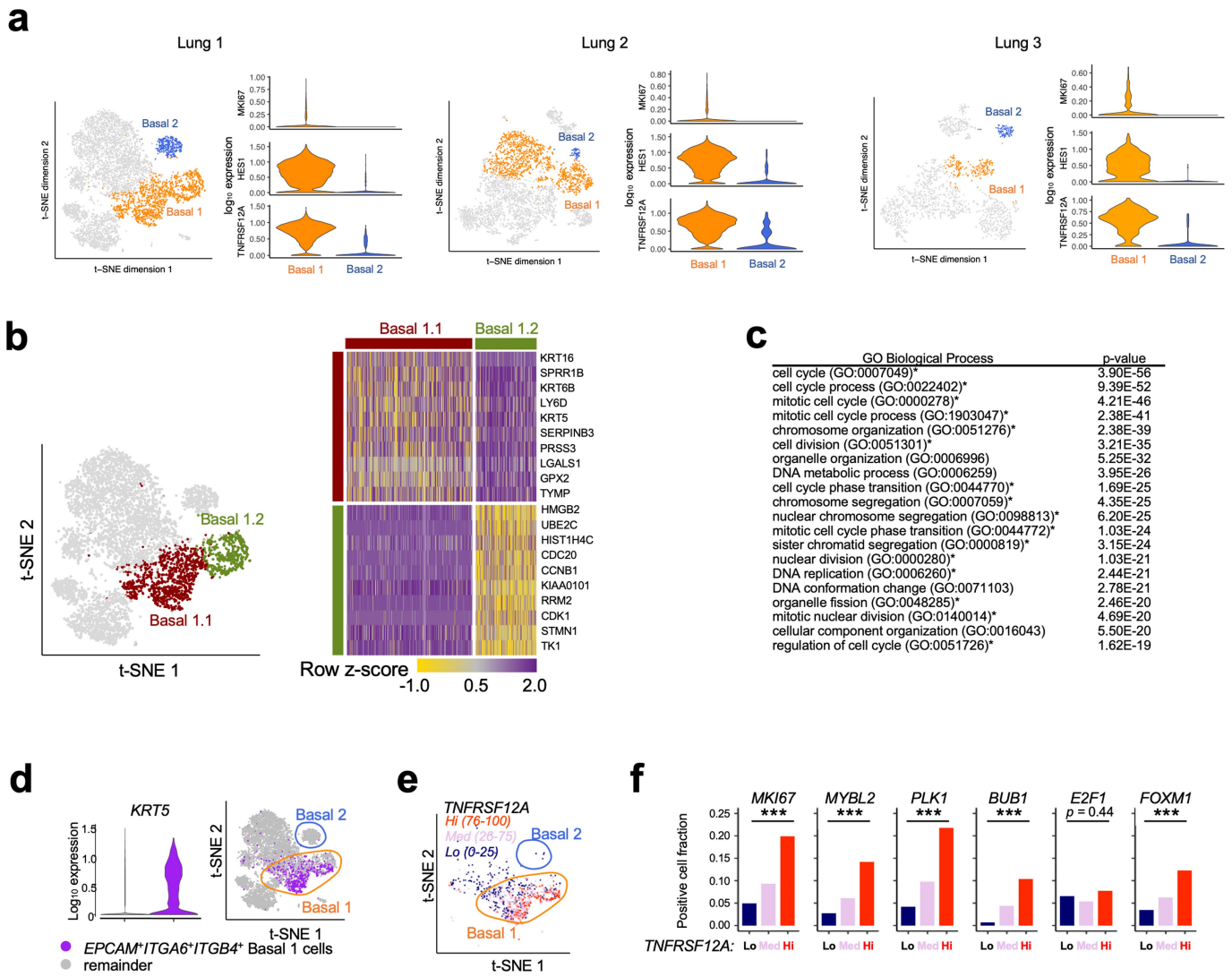

Extended Data Fig. 6 | scRNA-seq identifies an active basal cell subpopulation across three individual patient organoid cultures. a, High resolution clustering analysis identifies a reproducible active basal cell subpopulation with significantly higher expression of mRNAs for *TNFRSF12A*, the NOTCH pathway marker *HES1*, and the proliferation marker *MKI67*. Modified Kruskal-Wallis Rank Sum Test two tail p-values: *TNFRSF12A* 4.15×10^{-8}; *HES1* 2.4×10^{-10}; *MKI67* 3.4×10^{-3}. **b**, Fine resolution clustering of KRT5$^+$ populations identifies two Basal 1 sub-clusters, Basal 1.1 and 1.2. **c**, Gene Ontology PANTHER overrepresentation of differentially expressed genes enriched in Basal 1.2 versus 1.1 show the majority of Basal 1.2 processes involve cell cycle (asterisks). Complete analysis is provided in Supplementary Table 3. **d**, Violin plot of scRNA-seq analysis for Fig. 2f-h depicting *KRT5* mRNA expression among triply *EPCAM*$^+$*ITGA6*$^+$*ITGB4*$^+$ mRNA-expressing single cells (purple, i.e. tandem mRNA expression of all three genes) versus the remainder of cells (gray), $p < 0.001$ two tailed Kruskal-Wallis Rank Sum Test. **e**, t-SNE visualization of *TNFRSF12A* and *ITGA6* expression from the left panel among cells with *EPCAM*$^+$*ITGA6*$^+$*ITGB4*$^+$ gene expression and subdivision by high (top quartile, orange), medium (pink) and low (bottom quartile, navy blue) mRNA expression. **f**, Proliferation-associated gene expression is progressively enriched for scRNA-seq cell fractions of in *EPCAM*$^+$*ITGA6*$^+$*ITGB4*$^+$ cells that are stratified for low, medium, or high expression of *TNFRSF12A* mRNA as in (e). Data in f represent cell population fractions from a single experiment. *** = $p < 0.001$, two tailed Chi-square test.

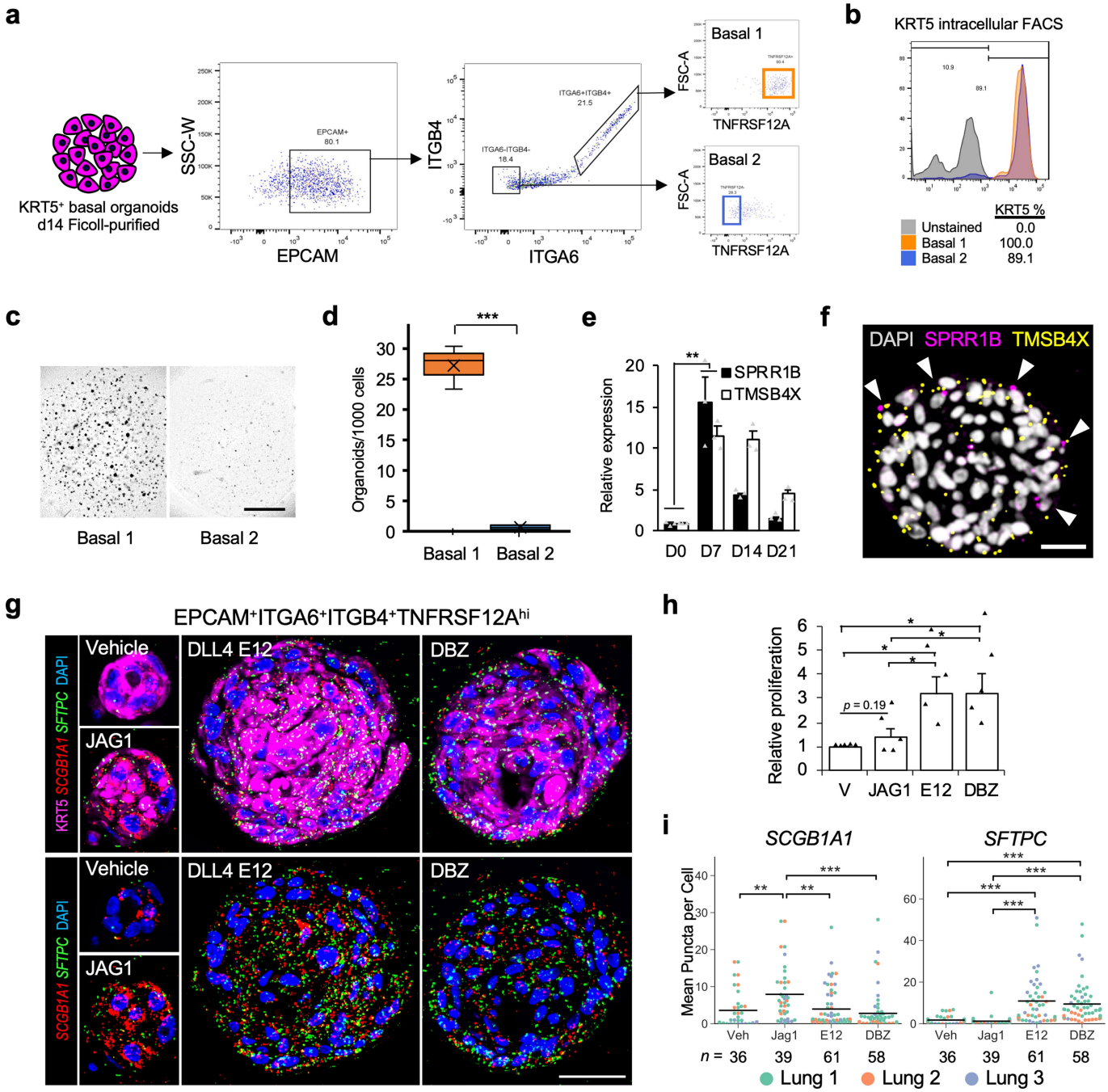

Extended Data Fig. 7 | Evaluation of Basal 1 lineage relationship to Basal 2 and the influence of NOTCH signaling on Basal 1 renewal and differentiation. a, Isolation of Basal 1 and Basal 2 via differential sedimentation of KRT5$^+$ cells followed by FACS sorting of EPCAM$^+$ITGA6$^+$ITGB4$^+$TNFRSF12A$^+$ (Basal 1) versus EPCAM$^-$ITGA6$^-$ITGB4$^-$TNFRSF12A$^-$ (Basal 2). **b**, Intracellular FACS measurement of KRT5 protein expression in Basal 1 and 2 fractions from (a). **c**, Representative brightfield of day 14 organoid cultures from (a-b). **d**, Quantitation of 3 independent experiments from (a-c), boxplot represents first quartile, median, third quartile, and whiskers represent minimum and maximum. *** $p < 0.001$, two tailed student's t-test. **e**, qPCR measurement of two differentially upregulated Basal 2 genes from the three scRNA-seq biological replicates (Extended Data Fig. 6, *SPRR1B*, *TMSB4X*) after prolonged culture of FACS isolated Basal 1 cells. Data are relative mean +/- SEM of cultures from three independent experiments, ** = $p < 0.01$, two tailed student's t-test. **f**, RNA FISH demonstrating *TMSB4X* and *SPRR1B* cellular transcripts within organoids originating from Basal 1 cells (arrows), scale bar = 25 µm. **g**, KRT5 immunostaining and *SFTPC* and *SCGB1A1* RNA FISH of FACS isolated TNFRSF12A^{hi} Basal 1 cells under vehicle, NOTCH agonism (JAG1 peptide), or NOTCH antagonism with the Delta-like ligand mutant 4 (DLL4^{E12}; E12) or the gamma secretase inhibitor DBZ; scale bar = 50 µm. **h**, Fluorescent quantitation of resazurin dye reduction to estimate relative cellular proliferation in (g), data are normalized to vehicle (V) and represent mean +/- SEM from five independent experiments, * $p < 0.05$, two tailed student's t-test. **i**, Quantitation of *SCGB1A1* and *SFTPC* gene expression by RNA FISH in the context of NOTCH agonism or antagonism from three independent experiments, ** $p < 0.01$, *** $p < 0.001$, two tailed student's t-test. *SFTPC* mRNA upregulation was not accompanied by lamellar body or SFTPC protein production (data not shown).

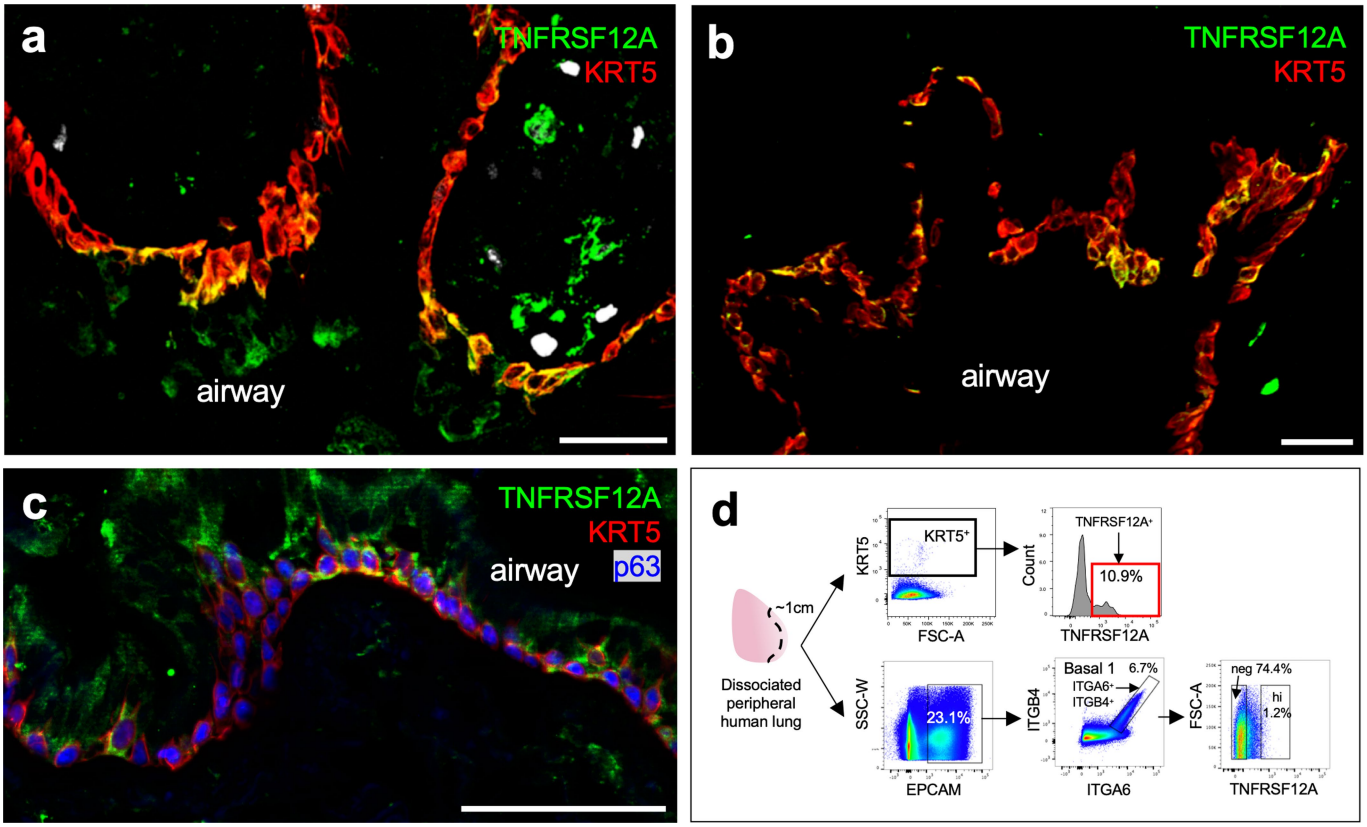

Extended Data Fig. 8 | TNFRSF12A marks a subset of distal airway basal cells *in vivo*. a-b, Immunostaining of KRT5 and TNFRSF12A in human distal airways from two individuals, scale bar = 100 µm. **c**, Immunostaining of KRT5, TNFRSF12A, and p63 in human distal airway, scale bar = 100 µm. **d**, FACS analysis from freshly fixed human distal lung with anti-KRT5 (intracellular) and monoclonal anti-TNFRSF12A (cell surface) (top), or sequential FACS isolation from freshly dissociated human distal lung of EPCAM+ITGA6+ITGB4+ cells followed by fractionation into TNFRSF12A^{hi} or TNFRSF12A^{neg} subsets (bottom), pre-gated on live singlets and used for culture experiments in Fig. 3d–e.

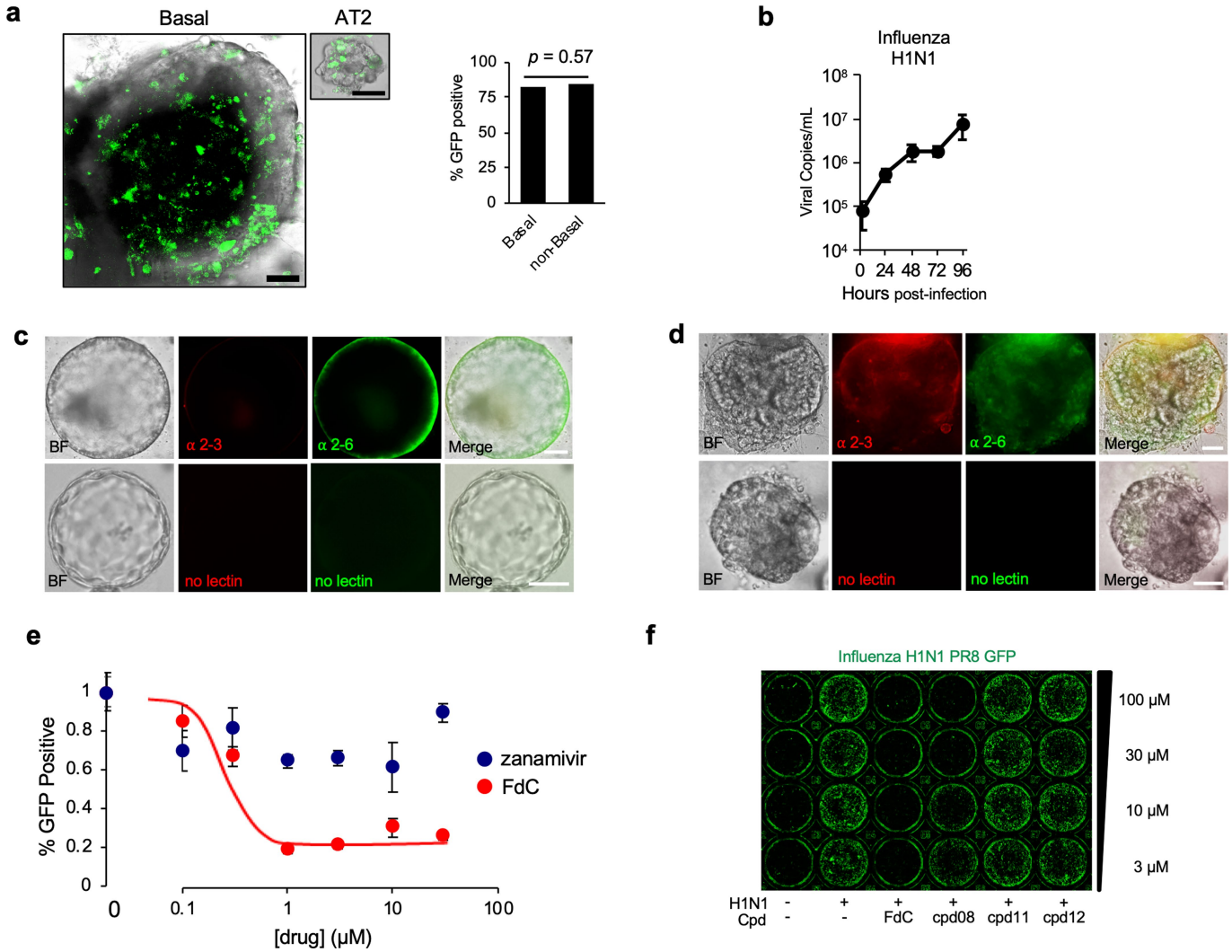

Extended Data Fig. 9 | Influenza infection modeling in mixed distal lung organoid cultures. a-b, Distal lung organoid modeling of H1N1 influenza infection. **a**, Merged transmission and GFP confocal images of purified basal (left) and purified AT2 organoids (right) 12 hours after infection with PR8-GFP H1N1 influenza virus, quantified by FACS for % GFP^+ cells. Bar plot represents the mean percentage of infected cells from three technical replicates, p = 0.57, Chi-square test. Scale bars = 50 μm. **b**, Viral genome quantitation over time of mixed distal lung organoid culture supernatants subjected to initial infection of wild-type H1N1 at an estimated multiplicity of infection (MOI) of 0.01, qRT-PCR, data represent the mean of three independent experiments +/- SEM. **c-d**, Lectin staining with *M. amurensis* (a2-3) and *S. nigra* (a2-6) lectins or no lectin negative controls to characterize sialic acid residues which serve as surface molecules for influenza virus host cell entry. AT2 organoids (c) and basal organoids (d). Scale bar = 25 μm. **e**, Dose response curves for two different classes of antiviral drugs on influenza infectivity and replication. The nucleoside analog FdC demonstrated dose dependent activity with IC_{50} of 340 nM as compared to neuraminidase inhibitor zanamivir, only impairs viral shedding, but not infectivity and replication. n = 3 per condition, data represents mean +/- SEM. **f**, Fluorescence micrograph of multiwell screening of selected various antiviral agents after H1N1 PR8-GFP organoid infection in 48 well format. FdC= nucleoside analog 2'-deoxy-2'-fluorocytidine. Cpd= compound #.

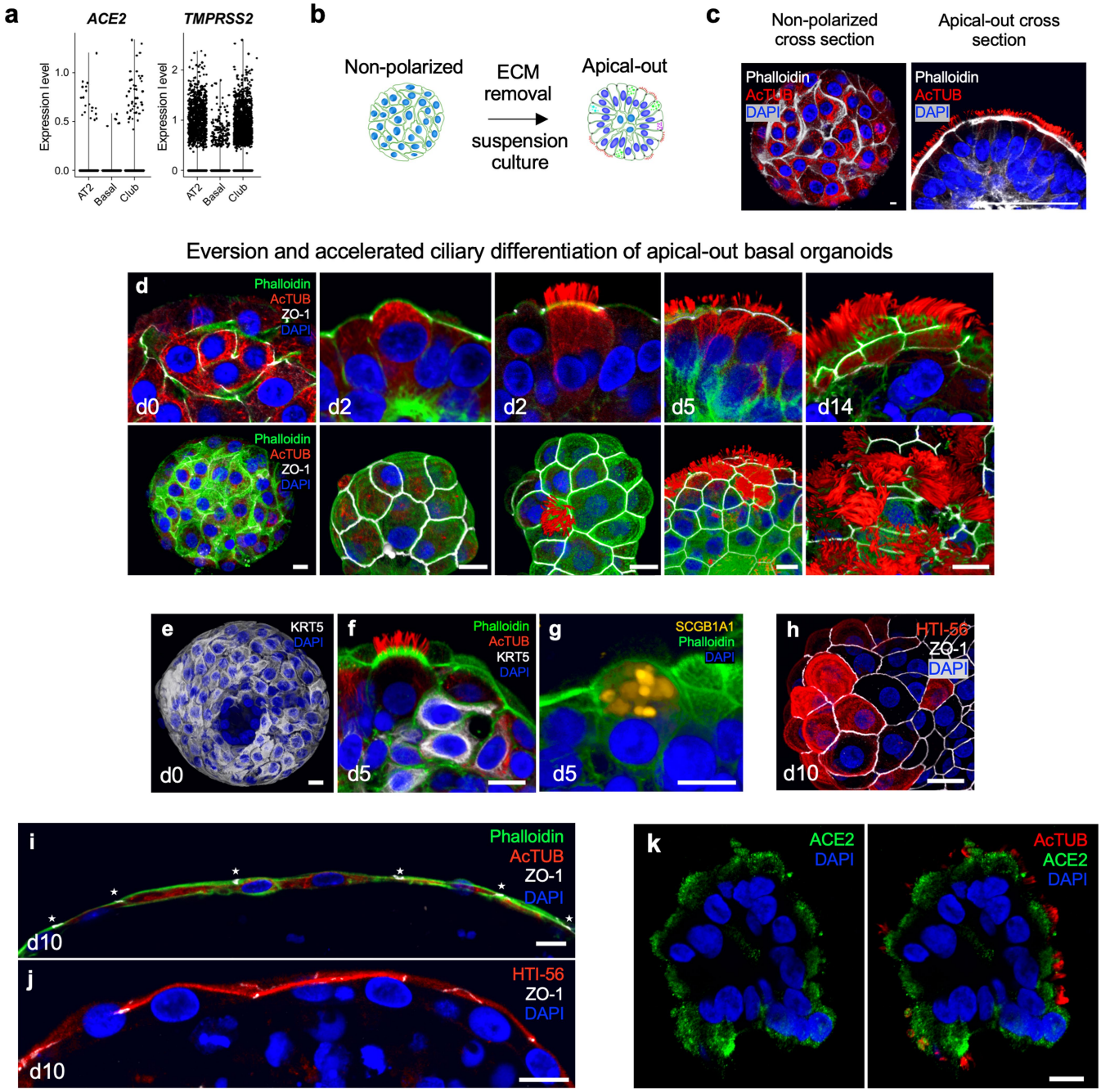

Extended Data Fig. 10 | Apical-out polarization and multi-lineage differentiation of distal lung organoids upon suspension culture. **a-b**, Formation of apical-out lung organoids. **a**, scRNA-seq plots of *ACE2* and *TMPRSS2* gene expression in non-everted mixed distal lung organoids as in Fig. 1a–h. **b**, Diagram of ECM removal and suspension culture leading to apical-out polarity of lung organoids. **c**, Representative confocal microscopy showing reorganization of microfilaments (phalloidin) and acetylated microtubules (AcTUB) upon ECM removal. Scale bar = 10 µm. **d-f**, Eversion and accelerated ciliary differentiation of apical-out basal organoids. **d**, Confocal 3D sections (top panels) and surface reconstructions (bottom panels) of apical-out lung organoids at different days after ECM removal. At day 0 (d0) microfilament (green, phalloidin) and microtubule (red, acetylated tubulin) organization is not polarized while junctional strands (ZO-1, white) are polarized. By day 2 in suspension (d2) ZO-1 (white) forms junctional rings in the apical periphery of each cell facing the external side of the organoids and the actin cytoskeleton forms microvilli (green) facing outward (apical-out polarity). Also at d2 some cells initiate microtubule polarization. By day 5 (d5) many more cells have motile cilia facing outwards. Mature motile cilia can be observed for several weeks, example at day 14 (d14). **e**, 3D confocal reconstruction of an organoid embedded in ECM consisting mostly of basal stem cells (KRT5$^+$, white). **f**, As apical-out polarity is established and ciliagenesis begins, KRT5$^+$ basal cells are found underneath the polarized epithelium. **g**, SCGB1A1$^+$ Club cells with apical-out polarity can are present on the exterior everted surface. In all panels nuclei are stained blue with DAPI, and actin microfilament organization visualized with phalloidin (green). Scale bars = 10 µm. **h-j**, Prolonged suspension culture of AT2 organoids (day 10 post-eversion) induces apical-out polarization and AT1 differentiation. **h**, Optical sections through alveolar-derived organoids after 10 days in suspension culture show decreased abundance of AT2 cells while individual cuboidal cells begin to express the AT1 marker HTI-56 (red), a transmembrane protein specific to the apical membrane of alveolar type 1 pneumocytes (AT1). Scale bars = 10 µm. **i-j**, Side views of alveolar organoids after 10 days of suspension culture reveal thin AT1 cells with phalloidin-reactive apical junctional complexes facing outwards (apical-out) (i) and expression of HTI-56 on the apical membrane (j). Scale bars = 10 µm. **k**, Representative confocal microscopy immunofluorescence of apical-out human basal organoid after 10 days in suspension expressing SARS-CoV-2 receptor ACE2 (green), cilia (AcTUB, red) and DAPI (blue). Scale bar = 20 µm.